ACS OMEGA

Open Access

http://pubs.acs.org/journal/acsodf

Article

Carbohydrazone/Thiocarbohydrazone-Based Dual-Responsive Probes for Highly Selective Detection of Cu^{2+}/Fe^{3+} Cations and F^-/ClO_4^- Anions, and Their Application in Bioimaging of Live Cells and Zebrafish Larvae

Ramalingam Gajendhiran, Abbas Khaja Raees Ahmed, Sivaraj Mithra, Seepoo Abdul Majeed, Azeez Sait Sahul Hameed, Kesavan Muthu, Sankar Sarathkumar, Selvan Nehru, and Aziz Kalilur Rahiman*

Cite This: *ACS Omega* 2024, 9, 50957−50977

Read Online

ACCESS | Metrics & More | Article Recommendations | Supporting Information

ABSTRACT: Four dual-responsive probe molecules 1,5-bis-(thiophene-2-carbaldehyde)carbohydrazone (R1), 1,5-bis-(thiophene-2-carbaldehyde)thiocarbohydrazone (R2), 1,5-bis-(indole-3-carbaldehyde)carbohydrazone (R3), and 1,5-bis(indole-3-carbaldehyde)thiocarbohydrazone (R4) were synthesized, characterized, and investigated for their sensing efficacy. The initial sensing behavior of the probes was tested by colorimetric signaling, followed by spectral and theoretical techniques, which supported the dual-sensing ability of the selected inorganic ions. The probes exhibited highly selective optical recognition for Cu^{2+}/Fe^{3+} cations and F^-/ClO_4^- anions compared to the tested cations and anions. Interestingly, the addition of Cu^{2+} and F^- ions to the probes resulted in "turn-on" fluorescence responses. Job's plot studies showed 1:2 stoichiometry between the probe molecules and cations and 1:1 stoichiometry between the probe molecules and anions. The binding constant of the probe molecules with the sensed ions was determined by the Benesi−Hildebrand equation and was found to be between 7.08×10^4 and 7.44×10^6 M^{-1} with a limit of detection between 0.11 and 0.80 μM, in CH_3CN:DMF (9:1, v/v). Density functional theory calculations established the nature of the interaction between the probe molecules and sensed ions. Further, the practical utility of the probes was successfully demonstrated with paper strip experiments, fluorescence imaging of Cu^{2+} ions in *Dr*G cells and zebrafish larvae, as well as in the development of molecular logic gates.

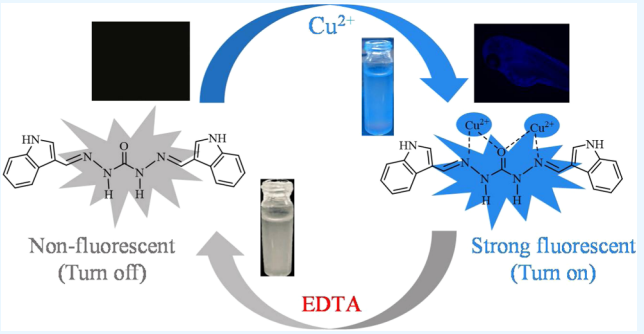

INTRODUCTION

The development of an effective approach for the detection and monitoring of toxic inorganic ions in environmental and biological systems is a major challenge for inorganic researchers. The detection of inorganic ions at trace levels can be inferred from the changes in color, wavelength, voltage, and other parameters when the analyte species interact with the sensor molecules. During the past few years, many synthetic probe molecules have been reported for sensing these ions. The incorporation of chromophores into the probe molecules may increase the sensitivity and decrease the limit of detection.[1,2] The visual-based sensors are considered a powerful sensing tool, which does not require any special instruments and can be detected by the naked eye even before the use of spectrophotometric analysis, despite the fact that the fluorescent sensors have been attracting the attention of chemosensor researchers.[3,4] The selectivity and sensitivity of sensor molecules are influenced by the solvent used and substitutional groups.[5]

The heavy inorganic metal ions and anions may contaminate environmental, industrial, and biological samples that pave the way for molecular recognition in the selective sensing of these ions.[6,7] For example, higher concentrations of Cu^{2+}/Fe^{3+} ions may cause serious health issues in humans such as Alzheimer's, Huntington's, Parkinson's, Menke's, and Wilson's diseases. According to the U.S. Environmental Protection Agency (EPA), the standard concentrations of Cu^{2+} and Fe^{3+} ions in drinking water are defined as 1.0 and 0.3 mg/L, respectively.[8,9] In inorganic anions, the F^- anion is one of the most important anions due to its ability to fight dental caries and its advantages

Received: April 26, 2024
Revised: October 10, 2024
Accepted: December 6, 2024
Published: December 18, 2024

when present within the permissible limit in drinking water. Fluorosis, acute kidney and stomach ailments, and other illnesses are brought on by a fluoride imbalance and may cause metabolic disorders, spotted teeth, and skeletal illnesses.[10] The American Dental Association (ADA) and the EPA recommended F^- anion concentrations of ∼0.6−1.2 and ∼2−4 mg/L in bottled water and drinking water, respectively. The perchlorate salts may also contaminate the environment due to their widespread use in automotive airbag systems, batteries, explosives, lubricants, paint production, pyrotechnics, solid rocket propellants, etc. Based on the recommendations of the National Academy of Sciences, the EPA has set a new limit of perchlorate to 15 μg/L in drinking water.[11,12] As a result, researchers have focused on developing new colorimetric and fluorometric devices to monitor these ions in order to avoid the ill effects on the human body due to their excessive concentration.

The design of sensor molecules with dual binding sites for the simultaneous detection of cations and anions under given physiological conditions is a burgeoning area of supramolecular chemistry due to their important role in biological, environmental, and industrial processes. The heteroaromatic thiophene family, which is electronically connected to the recognition sites, is an efficient π-conjugated system.[6] Similarly, indole and related heterocycles containing relatively acidic hydrogen atoms may act as components of neutral anion-receptor systems, could be widely used for the formation of complexes with ions, and are rapidly emerging as an important new class of ion-binding agents.[13] Indole-based probes exhibited high selectivity in their anion-binding capability and also served as dual-channel sensors.[14] In addition, carbohydrazone/thiocarbohydrazone-containing π-conjugated heterocyclic derivatives are appropriate systems for the colorimetric and fluorometric sensing of inorganic ions.[1,15] These sensors utilize various types of signaling mechanisms, including excited-state proton transfer (ESPT), internal charge transfer (ICT), and photoinduced electron transfer (PET).[16]

In the current context, the quintessential scope of many researchers is to develop colorimetric and fluorometric chemosensors capable of recognizing and detecting different analytes with high binding constants and low detection limits. Therefore, we constructed four dual-responsive carbohydrazone/thiocarbohydrazone-based probe molecules 1,5-bis(thiophene-2-carbaldehyde)carbohydrazone (R1), 1,5-bis(thiophene-2-carbaldehyde)thiocarbohydrazone (R2), 1,5-bis(indole-3-carbaldehyde)carbohydrazone (R3), and 1,5-bis(indole-3-carbaldehyde)thiocarbohydrazone (R4) for the detection of inorganic cations and anions in an organic medium. The fluorescent behavior of these probe molecules toward Cu^{2+} ions was successfully demonstrated in live-cell imaging studies using the *DrG* cell lines *in vitro* and zebrafish (*Danio rerio*) larvae as *in vivo* vertebrate model systems. To broaden its practical applicability, we extended our investigation to paper strips and molecular logic gate studies.

EXPERIMENTAL SECTION

Materials and Methods. Thiophene-2-carbaldehyde, indole-3-carbaldehyde, carbohydrazide, and thiocarbohydrazide were obtained from Sigma-Aldrich and were used as received. HPLC-grade acetonitrile, diethyl ether, dimethylformamide, dimethyl sulfoxide, ethanol, and methanol were purchased from AVRA Chemicals (India). Chloride salts of cations, such as K^+, Mg^{2+}, Ca^{2+}, Mn^{2+}, Fe^{3+}, Co^{2+}, Ni^{2+}, Cu^{2+}, and Zn^{2+}, were purchased from Merck Chemicals, while tetrabutylammonium (TBA) salts of anions, such as F^-, Cl^-, Br^-, I^-, HSO_4^-, ClO_4^-, NO_3^-, and OH^-, were obtained from AVRA Chemicals (India) and used as received. The melting points were measured using an electrothermal capillary apparatus and are reported as uncorrected values. CHN elemental analyses were carried out using a Carlo Erba Model 1106 elemental analyzer. Fourier transform infrared (FT-IR) spectra were recorded on a PerkinElmer FT-IR LX-185256 spectrophotometer between 4000 and 400 cm^{-1}. The UV−vis spectra were recorded on a PerkinElmer Lamda-25 UV−vis spectrophotometer. Fluorescence spectra were recorded on a Horiba FluoroMax Plus R928P 1700 nm emission spectrofluorometer. A Qtof Micro YA263 TOF mass spectrometer was used to record the ESI-LCMS mass spectra. Bruker advance 500 and 400 MHz spectrometers were used to record ^1H and ^{13}C NMR spectra, respectively, in DMSO-d_6 with tetramethylsilane (TMS) as an internal standard at ambient temperature. Chemical shifts are expressed in δ ppm units.

Synthesis of Dual-Responsive Probe Molecules (R1−R4). *Synthesis of 1,5-Bis(thiophene-2-carbaldehyde)-carbohydrazone (R1).* An ethanolic solution (20 mL) of thiophene-2-carbaldehyde (0.224 g, 2 mmol) was slowly added to an aqueous solution (20 mL) of carbohydrazide (0.090 g, 1 mmol) in acetic acid (2 drops) as the catalyst with constant stirring. After complete addition, the reaction mixture was refluxed by stirring for 24 h. The precipitate formed was cooled to room temperature, filtered, washed with ethanol and diethyl ether, and dried. Yield: 0.34 g (89%). Color: pale brown. M.p.: 178 °C. Anal. Calcd for $C_{11}H_{10}N_4OS_2$ (FW: 278.33, g/mol): C, 47.46; H, 3.62; N, 20.13. Found: C, 47.18; H, 3.84; N, 19.86 (%). FT-IR data (υ/cm^{-1}): 3088 υ(N−H), 1676 (C═O), 1610 (C═N). UV−vis [λ_{max} (nm) (ε, M^{-1} cm^{-1})] in CH_3CN: 278 (3202), 310 (4578). ^1H NMR (500 MHz, DMSO-d_6, δ ppm): 10.59, 10.39 (s, 2H, N−NH), 8.37, 8.10 (s, 2H, HC═N), 7.67−7.32 (m, 6H, thiophene−H). ^{13}C NMR (400 MHz, DMSO-d_6, δ ppm): 159.53 (C═O), 158.65, 156.05 (C═N), 127.51−115.23 (aromatic C). ESI-LCMS: 279.00 $[C_{11}H_{10}N_4OS_2]^+$, 127.00 $[C_5H_7N_2S]^+$.

Synthesis of 1,5-bis(thiophene-2-carbaldehyde)-thiocarbohydrazone (R2). The dual-responsive probe molecule R2 was synthesized using the same procedure as that for probe R1 using thiocarbohydrazide (0.106 g, 1 mmol) instead of carbohydrazide. Yield: 0.32 g (88%). Color: yellowish brown. M.p.: 180 °C. Anal. Calcd for $C_{11}H_{10}N_4S_3$ (FW: 294.39, g/mol): C, 44.88; H, 3.42; N, 19.03. Found: C, 45.05; H, 3.11; N, 19.48 (%). FT-IR data (υ/cm^{-1}): 3057 υ(N−H), 1604 (C═N), 738 (C═S). UV−vis [λ_{max} (nm) (ε, M^{-1} cm^{-1})] in CH_3CN: 340 (5753). ^1H NMR (500 MHz, DMSO-d_6, δ ppm): 11.64, 11.58 (s, 2H, N−NH), 10.46, 9.08 (s, 2H, HC═N), 7.24−7.19 (m, 6H, thiophene−H). ^{13}C NMR (400 MHz, DMSO-d_6, δ ppm): 176.67 (C═S), 140.65 (C═N), 127.88−115.35 (aromatic C). ESI-LCMS: 295.00 $[C_{11}H_{10}N_4S_3]^+$, 184.00 $[C_6H_6N_3S_2]^+$, 169.00 $[C_6H_6N_2S_2]^+$, and 127.00 $[C_5H_7N_2S]^+$.

Synthesis of 1,5-bis(indole-3-carbaldehyde)-carbohydrazone (R3). The dual-responsive probe molecule R3 was synthesized using the same procedure as that for probe R1 using indole-3-carbaldehyde (0.290 g, 2 mmol) instead of thiophene-2-carbaldehyde. Yield: 0.30 g (78%). Color: pale yellow; m.p.: 245 °C. Anal. Calcd for $C_{19}H_{16}N_6O$: (FW: 344.34, g/mol): C, 66.27; H, 4.68; N, 24.40. Found: C, 66.98; H, 4.13; N, 23.97 (%). FT-IR data (υ/cm^{-1}): 2921 υ(N−H), 1648 υ(C═O), 1608 υ(C═N). UV−vis [λ_{max} (nm) (ε, M^{-1} cm^{-1})]

https://doi.org/10.1021/acsomega.4c04001
ACS Omega 2024, 9, 50957−50977

in CH_3CN: 318 (7466). ^1H NMR (500 MHz, DMSO-d_6, δ ppm): 11.69, 11.50 (s, 2H indole−NH), 10.30, 10.07 (s, 2H, N−NH), 8.92 (s, 2H, HC═N), 8.36−7.18 (m, Ar−H). ^{13}C NMR (400 MHz, DMSO-d_6, δ ppm): 165.58 (C═O), 163.94, 160.39 (C═N), 143.06−131.14 (aromatic C).

Synthesis of 1,5-bis(indole-3-carbaldehyde)-thiocarbohydrazone (R4). The dual-responsive probe molecule R4 was synthesized using the same procedure as that for probe R1 using indole-3-carbaldehyde (0.290 g, 2 mmol) and thiocarbohydrazide (0.106 g, 1 mmol) instead of thiophene-2-carbaldehyde and carbohydrazide, respectively. Yield: 0.38 g (81%). Color: pale yellow; m.p.: 249 °C. Anal. Calcd for $C_{19}H_{16}N_6S$: (FW: 360.95, g/mol): C, 63.31; H, 4.47; N, 23.32. Found: C, 62.94; H, 4.17; N, 23.14 (%). FT-IR data (υ/cm^{-1}): 2977 υ(N−H), 1601 (C═N), 724 υ (C═S). UV−vis [λ_{max} (nm) (ε, M^{-1} cm^{-1})] in CH_3CN: 353 (9276). ^1H NMR (500 MHz, DMSO-d_6, δ ppm): 11.81, 11.44 (s, 2H indole−NH), 9.43, 9.37 (s, 2H, N−NH), 8.68 (s, 2H, HC═N), 7.86−7.19 (m, Ar−H). ^{13}C NMR data (400 MHz, DMSO-d_6, δ ppm): 177.66 (C═S), 142.17 (C═N), 134.49−131.52 (aromatic C).

Chromogenic and Fluorogenic Detection of Cations and Anions. The recognition efficacy of the synthesized probe molecules toward various cations and anions was investigated in CH_3CN:DMF (9:1, v/v) solution. Titration experiments were carried out using chloride salts of cations (K^+, Mg^{2+}, Ca^{2+}, Mn^{2+}, Fe^{3+}, Co^{2+}, Ni^{2+}, Cu^{2+}, and Zn^{2+}) and TBA salts of anions (F^-, Cl^-, Br^-, I^-, HSO_4^-, ClO_4^-, NO_3^-, and OH^-). For optical sensing studies, a 1 μL aliquot of the cationic or anionic (2.5×10^{-4} M) solution was added to 2 mL solution of the probes (R1 and R3 = 2.5×10^{-5}, and R2 and R4 = 5×10^{-5}). The apparent binding constants (K_a) for the formation of different probes and ions (R1−R4 + ions) were evaluated using the Benesi−Hildebrand (B−H) equation from UV−vis absorbance as well as fluorescence titrations data, using the following equations

$$1/(A - A_0) = 1/(A_1 - A_0) + 1/(A_1 - A_0)K_a[\text{ion}]^m \quad (1)$$

$$1/(I - I_0) = 1/(I_1 - I_0) + 1/(I_1 - I_0)K_a[\text{ion}]^m \quad (2)$$

where $[\text{ion}]^m$ is the concentration of metal ions or anions, A_0 is the maximum absorbance of the probe molecules (R1−R4) obtained at a particular wavelength, A is the absorbance of the probes in the presence of a particular concentration of ions, and A_1 is the maximum absorbance of R1−R4 in the presence of excess ions. Similarly, I_0 is the emission intensity of the probe molecules in the absence of ions, I is the emission intensity of the probes in the presence of intermediate concentrations of the ions, and I_1 is the maximum emission intensity of the probe molecules in the presence of excess ions.[17]

The detection limit (LOD) was determined using the following equation

$$\text{LOD} = 3\sigma/m \quad (3)$$

where σ represents the standard deviation (SD) of the regression line, and m is the slope of the calibration line. To obtain the slope, the absorbance intensity was plotted as a function of the concentration of probes.[4,17] The binding stoichiometric ratio of the probe molecules with the sensed cations and anions was determined by Job's plot, using UV−vis absorbance titrations, keeping the total volume of the solution constant (2 mL) and changing the molar ratio of ions from 0.1 to 0.9.[18]

The fluorescence quantum yield (Φ) of probe R1 and its complexes (R1 + Cu^{2+}/F^-) were determined using quinine sulfate (literature quantum yield is 0.54) as a reference in 0.1 M H_2SO_4, according to the following equation:

$$\Phi_s = \Phi_r \times \frac{I_s}{I_r} \times \frac{A_r}{A_s} \times \left(\frac{\eta_s}{\eta_s}\right)^2 \quad (4)$$

where Φ is the quantum yield, I is the integrated area under the fluorescence spectra, A is the absorbance, η is the refractive index of the solvent, and subscripts s and r denote the sample and reference, respectively. The same excitation wavelength and bandwidth were applied to the sample and reference.

To ascertain the practical application of the synthesized probe molecules, paper strip experiments were carried out according to the previously described procedure.[19]

Theoretical Studies. The ground state (S_0) geometries of probe molecules (R1−R4) and their complexes were investigated using density functional theory (DFT) calculations and the Gaussian 03 program with the B3LYP/6-31+G(d,p) and B3LYP/LanL2DZ basis set.[4,20]

Bioimaging Studies. *Cell Culture.* The *Danio rerio* gill (*Dr*G) cells were obtained from the Access Center of National Repository for Fish Cell Lines (AC-NRFC), C. Abdul Hakeem College, Tamil Nadu, India, and cultured in Leibovitz's L-15 (GIBCO) medium containing the antibiotics fungizone (2.5 μg mL^{-1}) and kanamycin (100 μg mL^{-1}) supplemented with 10% fetal bovine serum (FBS). The *Dr*G cells were maintained at 28 °C in a BOD incubator.

In Vitro Morphological Changes in the Danio rerio gill (DrG) Cell Line. *Dr*G cells were plated into a 6-well tissue culture plate at a density of 2×10^5 cells (in 1.5 mL growth medium). The supernatants from the culture plates were removed after overnight growth, and fresh aliquots of growth medium containing five different concentrations (0, 5, 10, 20, 40, and 80 μM mL^{-1}) of the probes (R1−R4) were added. After 24 h of incubation, the cells were washed with phosphate-buffered saline (PBS, pH 7.4), and the morphological changes were examined under an inverted phase-contrast microscope at 100× magnification (Carl Zeiss, Germany).

In Vitro Cytotoxicity Assays. The *Dr*G cells were split and plated in 96-well tissue culture plates at a density of 5×10^5 cells mL^{-1}, and the sealed plates with *Dr*G cells were incubated for 24 h before exposure to the probes (R1−R4). Five different concentrations of probe molecules, prepared as described above, were added to eight replicates, and the cells were incubated for another 24 h. Two endpoints for the cytotoxicity assays (MTT and neutral red (NR)) were determined after 24 h of exposure. Cytotoxicity was determined in at least three independent experiments with eight replicates. Cell viability was expressed as a fraction of the negative control (cells treated with the medium alone).

MTT Assay. The MTT assay hinges on the uptake of 3-(4,5-dimethylthiazol-2-yl)-2,5-diphenyltetrazolium bromide (MTT) and its reduction in the mitochondria of viable cells to produce MTT formazan, whereas the dead cells were mostly negative in this cleavage activity.[21] Following a 24 h exposure to different concentrations of the probes (R1−R4), 20 μL of MTT solution (5 mg mL^{-1} in PBS buffer) was added to each well. After incubating the 96-well tissue culture plates for 4 h, excess MTT solution was removed from each well, followed by the addition of DMSO (200 μL) solution to individual wells. After 10 min of shaking at 450 rpm, 25 μL of Sorensen's glycine buffer (50 mM glycine, 50 mM NaCl/NaOH, pH 10.5) was added, the absorbance of each well was measured at 490 nm using a

https://doi.org/10.1021/acsomega.4c04001
ACS Omega 2024, 9, 50957−50977

Scheme 1. Synthesis of Dual-Responsive Sensor Molecules (R1−R4)

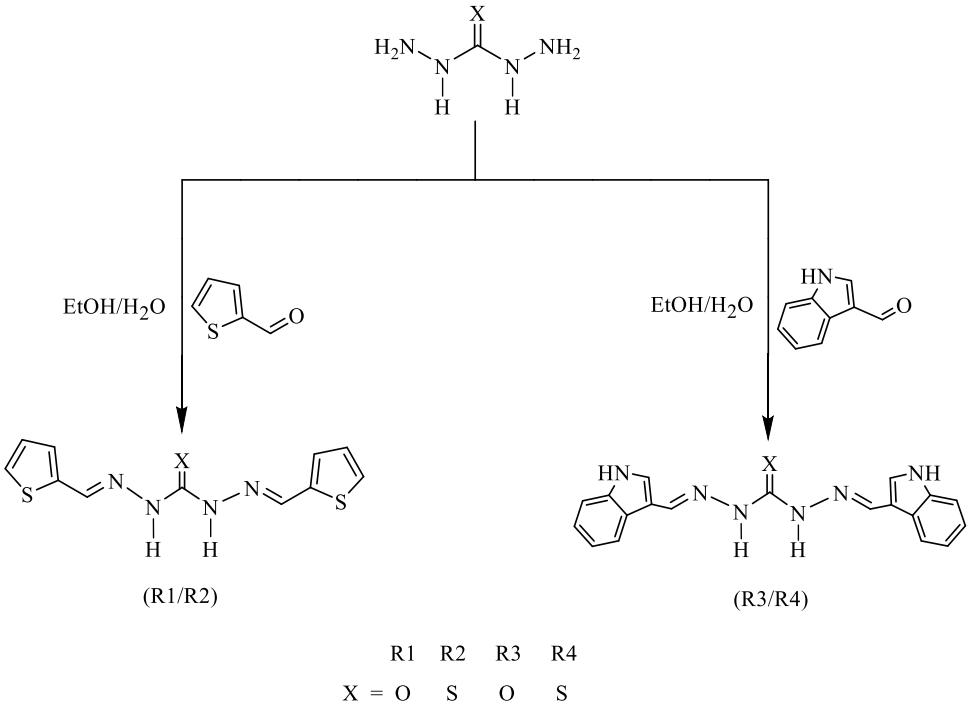

microplate reader (Thermo Electron Corporation, Japan), and the EC_{50} values were determined.

NR Assay. The NR (neutral red) assay is based on the uptake and accumulation of NR in living cells. The damaged cells can alter the uptake rates, whereas the dead cells cannot retain the dye.[22,23] The detailed procedure for the NR assay is described in the literature.[24] The *Dr*G cells were exposed to probe molecules (R1−R4) for 24 h, and the cells were washed with PBS followed by the addition of 200 μL of NR (50 μg mL^{-1} in medium) to each well. After the mixture was incubated for 3 h, excess solution was discarded. The NR dye taken up by *Dr*G cells was extracted and dissolved in isopropanol, and the absorbance of each plate was measured at 540 nm by using a microplate reader.

Cellular Imaging. The 6-well culture plates were used to seed and cultivate *DrG* cells. After confluence, the cells were switched to serum-free L-15 medium with Cu^{2+} ions (20 μM) and incubated for 30 min, and three PBS washes lasting 5 min each were performed. After 30 min, probe molecules (R1−R4) at concentrations of 10 and 20 μM were added to the designated wells and incubated for another 30 min. Finally, the cells were washed three times for 5 min each with PBS, and the images were captured using a fluorescence microscope (Carl Zeiss, Germany) at 100× magnification.[25]

In Vivo Tracing of Cu^{2+} Ions in Newly Hatched Zebrafish Larvae. The zebrafish were kept at 28 ± 2 °C and maintained under optimal breeding conditions. For mating, male and female zebrafish were maintained in the same tank at 28 ± 2 °C on a 12 h light/12 h dark cycle, and then, the spawning of eggs was triggered by light stimulation. E3 embryo medium was used to nurture the zebrafish larvae. Newly hatched zebrafish larvae were exposed to Cu^{2+} ions (20 μM) in aqueous solution for 30 min at 28 ± 2 °C. The solution was then removed, and the larvae were rinsed with deionized water (2 mL) three times to eliminate the unbound Cu^{2+} ions. Then, the larvae were incubated for 30 min with aqueous solutions containing 10 and 20 μM probe molecules (R1−R4) at 28 ± 2 °C, and the E3 solution was then removed. After three washes with deionized water (2 mL), the images of larvae were captured using a fluorescence microscope (40× magnification).[26] In the present study, all animal experiments were carried out in accordance with the guidelines and approval of the Committee for the Purpose of Control and Supervision of Experiments on Animals (1011/PO/Re/S/06/CPCSEA), Ministry of Environment and Forests, Government of India. All efforts were made to minimize suffering.

RESULTS AND DISCUSSION

Synthesis of Dual-Responsive Probe Molecules (R1−R4). The dual-responsive probe molecules 1,5-bis(thiophene-2-carbaldehyde)carbohydrazone (R1), 1,5-bis(thiophene-2-carbaldehyde)thiocarbohydrazone (R2), 1,5-bis(indole-3-carbaldehyde)carbohydrazone (R3), and 1,5-bis(indole-3-carbaldehyde)thiocarbohydrazone (R4) were synthesized by a simple Schiff base condensation reaction between thiophene-2-carbaldehyde/indole-3-carbaldehyde and carbohydrazide/thiocarbohydrazide (Scheme 1). All of the probes were soluble in CH_3CN, DMF, and ethyl alcohol. The structures of the probe molecules were characterized by elemental analysis, FT-IR spectroscopy, UV−vis absorption, ^1H and ^{13}C NMR, and ESI-LCMS spectral studies.

Spectral Characterization. The formation of dual-responsive probes (R1−R4) by the condensation reaction was supported by FT-IR spectral analysis (Figure S1). The disappearance of the aldehyde peak of thiophene-2-carbaldehyde at 1660 cm^{-1} and indole-3-carbaldehyde at 1636 cm^{-1} with the presence of a new azomethine υ(C═N) stretching peak at 1601−1610 cm^{-1} indicated the formation of probe molecules due to the Schiff base reaction. The bands corresponding to υ(N−H) were obtained at 2921−3088 cm^{-1}. Probes R1 and R3 showed the stretching vibration owing to υ(C═O) at 1676 and 1648 cm^{-1}, whereas R2 and R4 showed bands at 738 and 724 cm^{-1} owing to υ(C═S), respectively. The UV−vis absorption

https://doi.org/10.1021/acsomega.4c04001
ACS Omega 2024, 9, 50957−50977

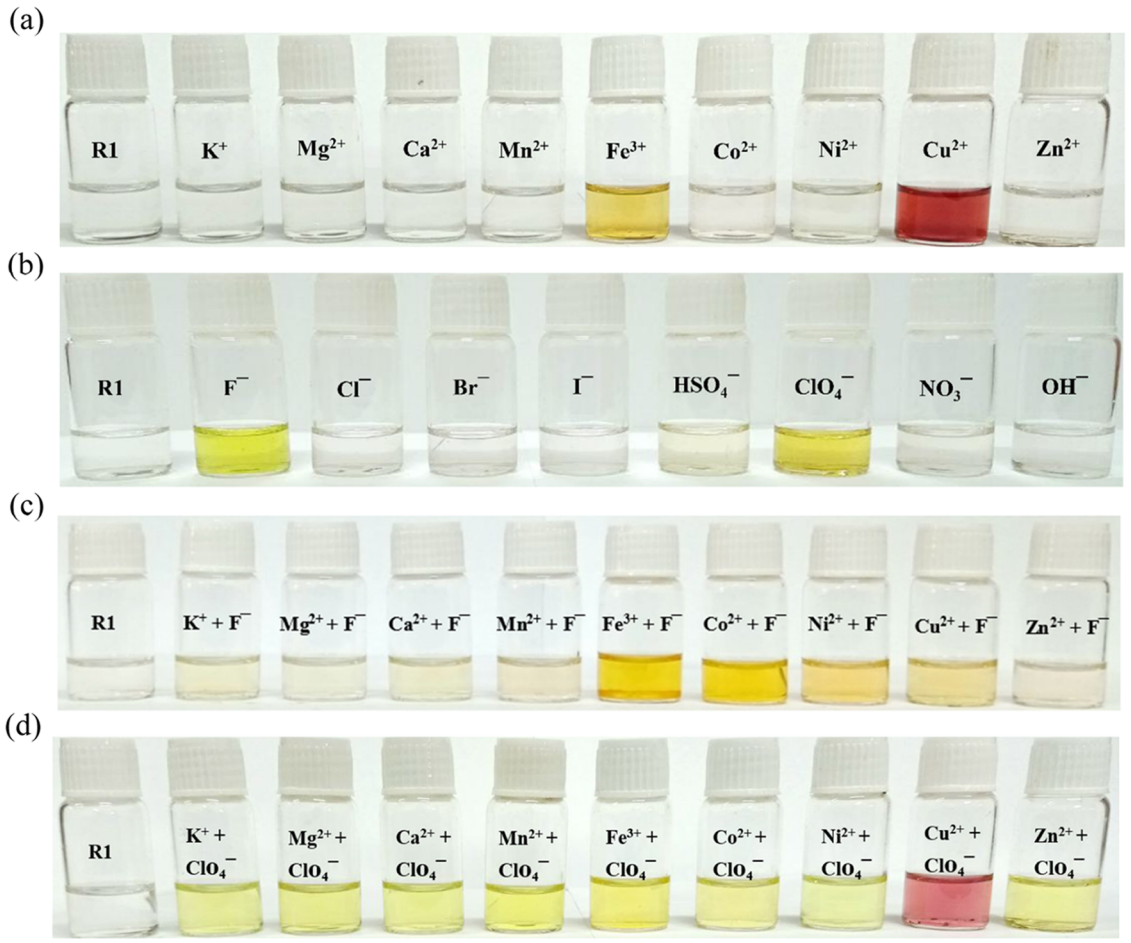

Figure 1. Visual detection of R1 with various cations (a), anions (b), simultaneous addition of cations followed by F^- anions (c), and simultaneous addition of cations followed by ClO_4^- anions (d) in CH_3CN:DMF (9:1 v/v) solution.

spectra of the dual-responsive probes showed a strong absorption band at 278−353 nm owing to intramolecular transitions (Figure S2).

The structures of the synthesized dual-responsive probe molecules were also confirmed by ^1H and ^{13}C NMR spectral studies (Figures S3−S6). The ^1H NMR spectra of the probes showed signals at 11.81−11.44, 11.64−9.37, 10.46−8.10, and 8.36−7.18 ppm, corresponding to indole −NH, NH, azomethine (CH═N), and aromatic protons, respectively. The ^{13}C NMR spectra of probes R1 and R3 displayed signals at 159.53 and 165.58 ppm corresponding to the carbon of the C═O group, while probes R2 and R4 exhibited signals at 176.67 and 177.66 ppm owing to the carbon of the C═S group, respectively. The C═N and aromatic carbon signals of the probe molecules were obtained at 163.94−140.65 and 143.06−115.23 ppm, respectively. ESI-LCMS spectra were also recorded to determine the stoichiometric composition of the synthesized probe molecules. The obtained molecular ion peak at m/z 278.00 and 295.00 due to $[C_{11}H_{10}N_4OS_2]^+$ and $[C_{11}H_{10}N_4S_3]^+$ corresponds to the molecular weight of the probe molecules R1 and R2, respectively (Figure S7). The various fragments observed for the probes with differing intensities at distinct m/z values were associated with the formation of the probe molecules (Figure S8). The observed mass spectral data supported the proposed molecular formulae of the synthesized probe molecules.

Sensor Properties of the Dual-Responsive Probes (R1−R4). *Colorimetric Responses with Cations and Anions.* The visual color change method is a simple and significant technique for optical sensing of different analytes. Hence, the naked-eye colorimetric responses of the synthesized dual binding probes (R1−R4) were carried out with the chloride salts of cations (K^+, Mg^{2+}, Ca^{2+}, Mn^{2+}, Fe^{3+}, Co^{2+}, Ni^{2+}, Cu^{2+}, and Zn^{2+}) and the TBA salts of anions (F^-, Cl^-, Br^-, I^-, HSO_4^-, ClO_4^-, NO_3^-, and OH^-) in an organic medium to observe the rapid detection of cations and anions, both separately and on the simultaneous addition of cations followed by anions (Figures 1 and S9−S11). The solution of probes, cations, and anions at concentrations 1.5×10^{-5}, 1.0×10^{-4}, and 2.5×10^{-5} M, respectively, were prepared in CH_3CN:DMF (9:1 v/v). The sensitivity and selectivity of the tested inorganic ions were assessed by adding a 1 μL aliquot of cationic or anionic solution to 2.5 mL of probe solutions. Distinct color changes were observed upon individual addition of Fe^{3+} and Cu^{2+} cations, F^- and ClO_4^- anions, and simultaneous addition of cations, followed by anions ($Fe^{3+} + F^-$, $Cu^{2+} + F^-$, $Fe^{3+} + ClO_4^-$, and $Cu^{2+} + ClO_4^-$) to the probe solutions. All four probe solutions were colorless. The interaction of Fe^{3+} ion with the probe molecules R1, R3, and R4 results in color changes from colorless to pale yellow, whereas R2 shows a brownish yellow color. The interaction of Cu^{2+} ions with R1−R4 results in color changes from colorless to reddish brown, yellow, pale yellow, and brown colors, respectively. The other cations tested did not show any

https://doi.org/10.1021/acsomega.4c04001
ACS Omega 2024, 9, 50957−50977

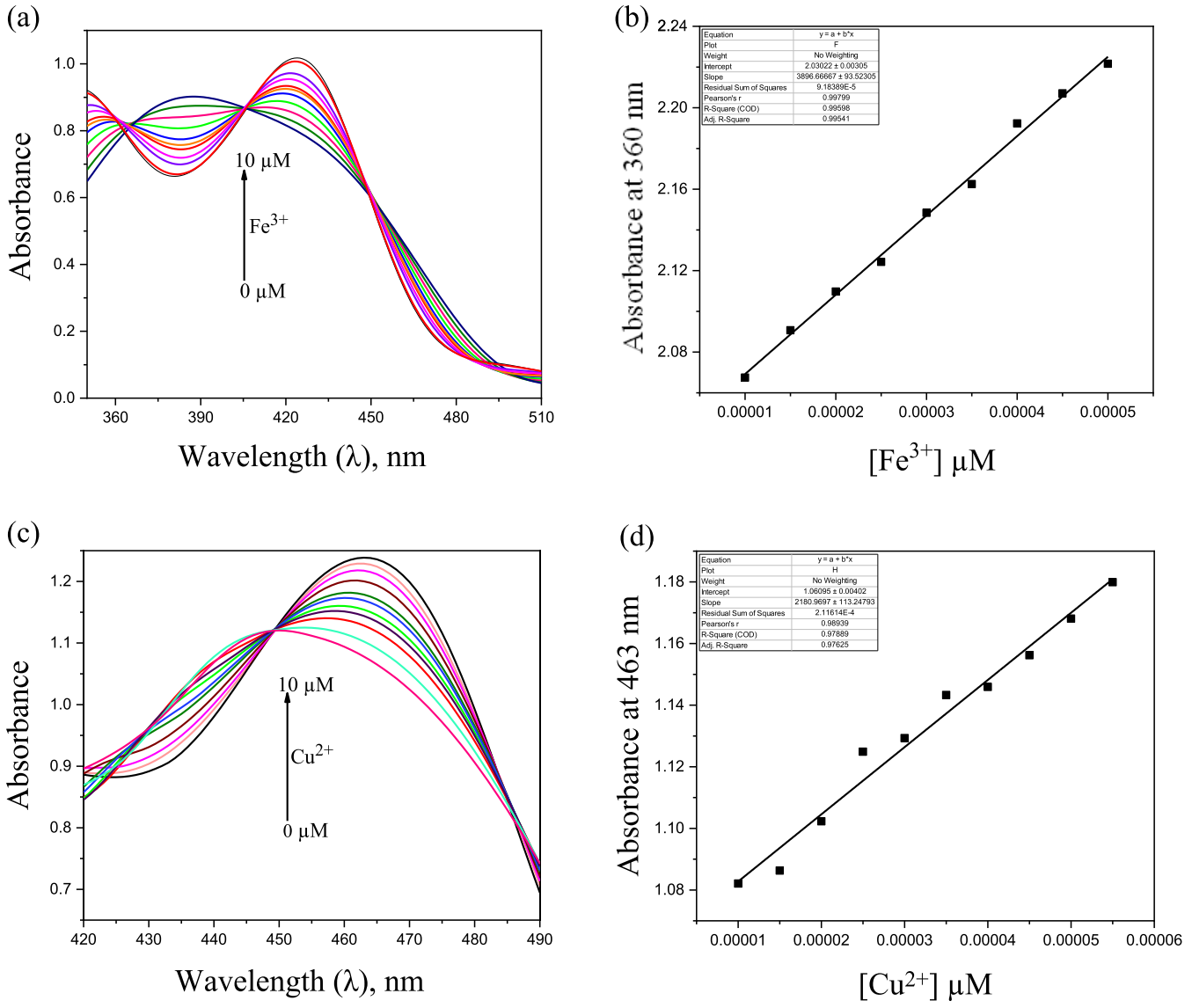

Figure 2. Absorption spectral titrations of probe R3 upon stepwise addition of Fe^{3+} (a) and Cu^{2+} (c) cations, and the corresponding calibration plots upon the addition of Fe^{3+} (b) and Cu^{2+} (d) cations.

detectable color changes with the probe molecules. Similarly, when the TBA salts of anions were individually added to the probes, only the F^- and ClO_4^- anions displayed rapid responses, whereas the other tested anions did not show any noticeable responses. The interaction of R1−R4 with the F^- anion results in a color change from colorless to greenish yellow for R1, R3, and R4, whereas R2 shows a pale brown color. The interaction of R1−R4 with the ClO_4^- anion results in a color change from colorless to yellow for R1, R3, and R4, whereas R2 shows a greenish yellow color. The occurrence of dramatic color changes signifies the hydrogen bonding interaction between the F^- and ClO_4^- anions and the −NH groups of the probe molecules.

The chromogenic detection ability of the probe molecules with respect to the simultaneous addition of sensed cations (Fe^{3+}/Cu^{2+}) followed by anions (F^-/ClO_4^-) was also analyzed. The simultaneous addition of the Fe^{3+} cations followed by the F^- anions to the probes (R1−R4) resulted in color changes from colorless to dark yellow and brownish yellow for R1 and R2, respectively, whereas no noticeable responses were observed for R3 and R4. The simultaneous addition of Fe^{3+} followed by ClO_4^- to R1−R4 showed no noticeable responses. Similarly, when the Cu^{2+} cation followed by F^- anion was added simultaneously to R1−R4, only R4 resulted in a color change from colorless to greenish gray, whereas the other probes did not show any noticeable responses. When the Cu^{2+} cation followed by ClO_4^- anion was added simultaneously to R1−R4, only R3 resulted in a color change from colorless to greenish gray, whereas the other probe molecules did not show any noticeable responses. The sensor molecules bearing the binding sites (−NH/O/N/S) are responsible for the coordination of cations and anions, and simultaneous sensing of both ions. The above colorimetric studies show that the probe molecules act as effective chromogenic sensors by the naked eye for individual as well as simultaneous detection of Fe^{3+}/Cu^{2+} cations and F^-/ClO_4^- anions, in which the dual binding behavior of the sensor molecules has been observed in a single molecule.

Absorption Responses with Cations and Anions. The UV−vis absorption titration experiments were performed to confirm the sensing behavior of the probe molecules (R1−R4) containing different binding sites (N/O/S). The binding

https://doi.org/10.1021/acsomega.4c04001
ACS Omega 2024, 9, 50957−50977

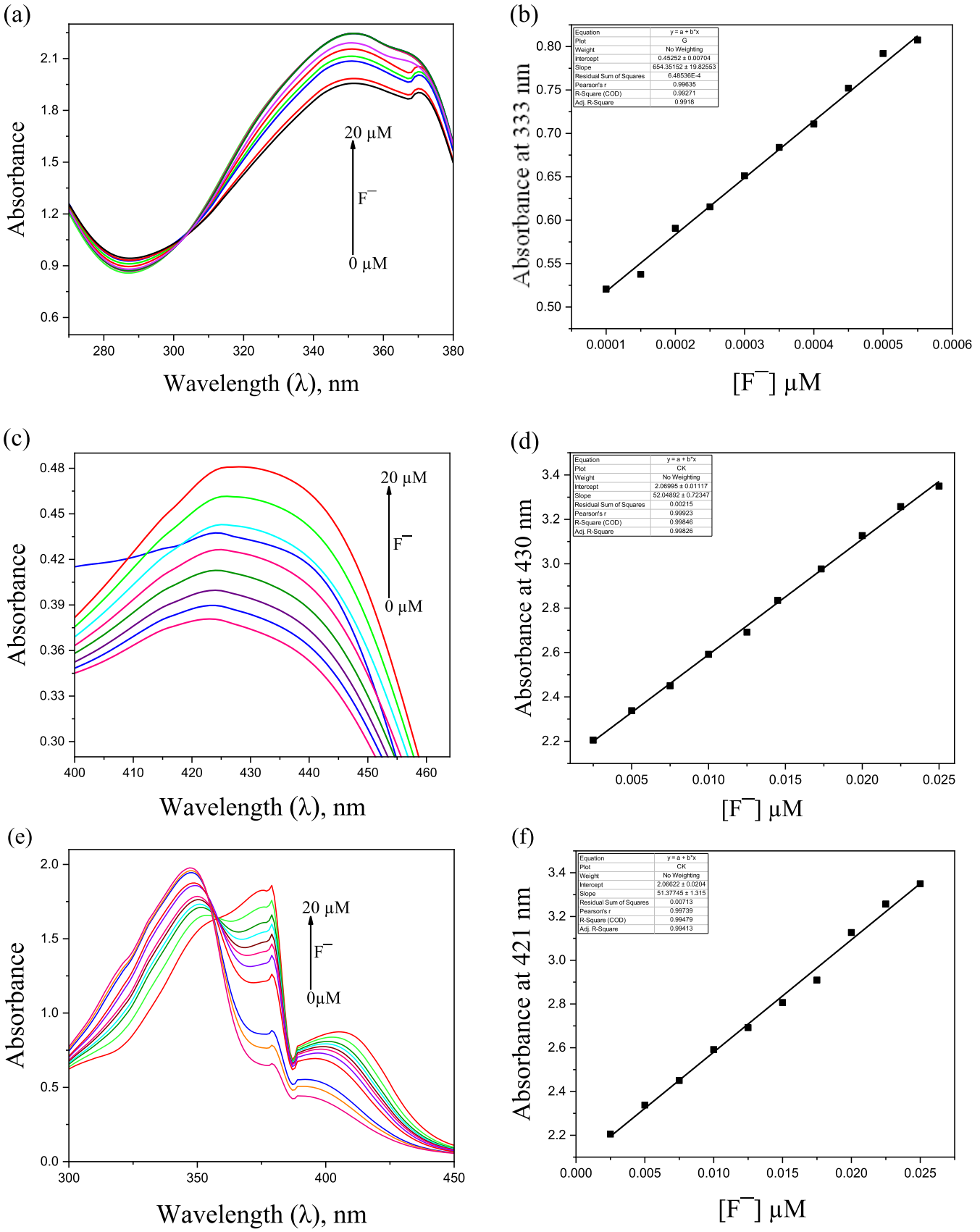

Figure 3. Absorption spectral titrations of probes R1 (a), R3 (c), and R4 (e) upon stepwise addition of F^- anions, and the corresponding calibration plots upon the addition of F^- anions to R1 (b), R3 (d), and R4 (f).

https://doi.org/10.1021/acsomega.4c04001
ACS Omega 2024, 9, 50957−50977

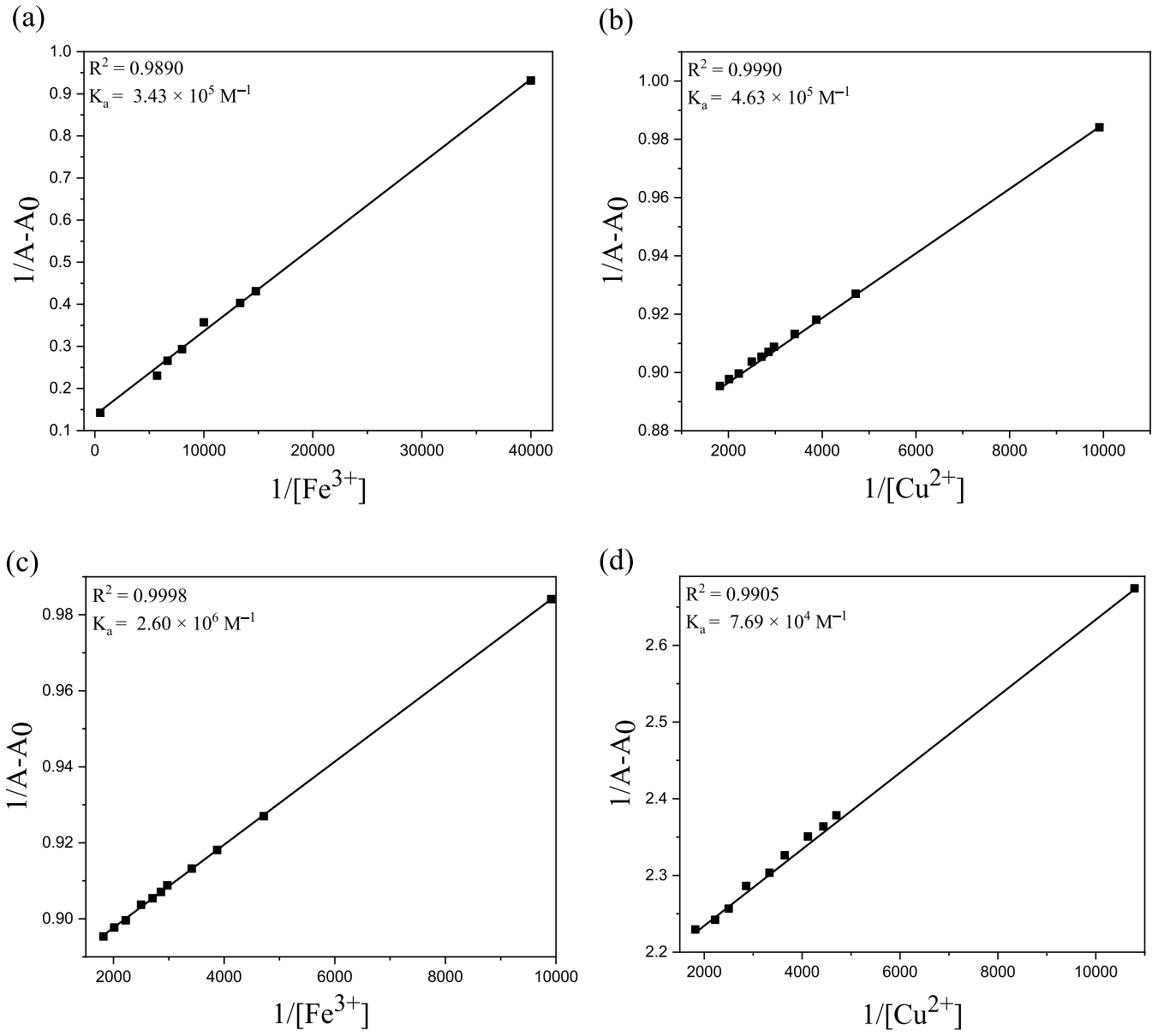

Figure 4. Benesi−Hildebrand plots for R1 with Fe^{3+} (a) and Cu^{2+} (b) cations, and R2 with Fe^{3+} (c) and Cu^{2+} (d) cations in a CH_3CN:DMF (9:1 v/v) solution to calculate the association constants by absorption titrations.

efficacy of R1−R4 with cations was analyzed by adding 2 μL of chloride salts of cations (K^+, Mg^{2+}, Ca^{2+}, Mn^{2+}, Fe^{3+}, Co^{2+}, Ni^{2+}, Cu^{2+}, and Zn^{2+}) and TBA salts of anions (F^-, Cl^-, Br^-, I^-, HSO_4^-, ClO_4^-, NO_3^-, and OH^-) in CH_3CN:DMF (9:1 v/v) solution with an analyte concentration of 2.5×10^{-5} M (Figures S12 and S13). The titration of probe molecules with cations and anions showed notable absorption changes with Fe^{3+}/Cu^{2+} and F^-/ClO_4^- ions due to the complexation of host−guest molecules, while the other cations and anions tested showed only negligible variations in intensity without any change in the peak positions. Upon the addition of the Fe^{3+} cation to probe R1, the intensity of the absorption bands at 278 and 310 nm increased with the appearance of a new band at 361 nm. The addition of the Fe^{3+} cations to R2 results in a bathochromic shift of 45 nm from 340 to 385 nm with increasing intensity. The addition of Fe^{3+} cations to R3 results in an increase in the intensity of the absorption band at 318 nm with the appearance of a new band at 360 nm, whereas the intensity of the absorption band at 353 nm decreases with the appearance of a new band at 407 nm for R4. The addition of Cu^{2+} cations to R1 results in an increase in the absorption intensity at 278 and 310 nm with the appearance of a new absorption band at 413 nm. The addition of Cu^{2+} cations to R2 results in a bathochromic shift of 43 nm from 340 to 383 nm with an increase in the absorption intensity and the appearance of a new band at 401 nm. The interaction of Cu^{2+} with R3 results in an increase in the absorption intensity at 318 nm with the appearance of a new band at 463 nm, whereas the intensity of the absorption band at 353 nm decreases with the appearance of two new bands at 401 and 464 nm for R4.

The addition of F^- anions to probe R1 results in an increase in the absorption intensity at 278 nm accompanied by a bathochromic shift of 90 nm from 310 to 400 nm, whereas R2 results in a decrease in the absorption intensity at 340 nm with the appearance of a new band at 436 nm. The addition of the F^- anions to R3 results in a bathochromic shift of 53 nm from 318 to 371 nm with the appearance of a new band at 430 nm,

https://doi.org/10.1021/acsomega.4c04001
ACS Omega 2024, 9, 50957−50977

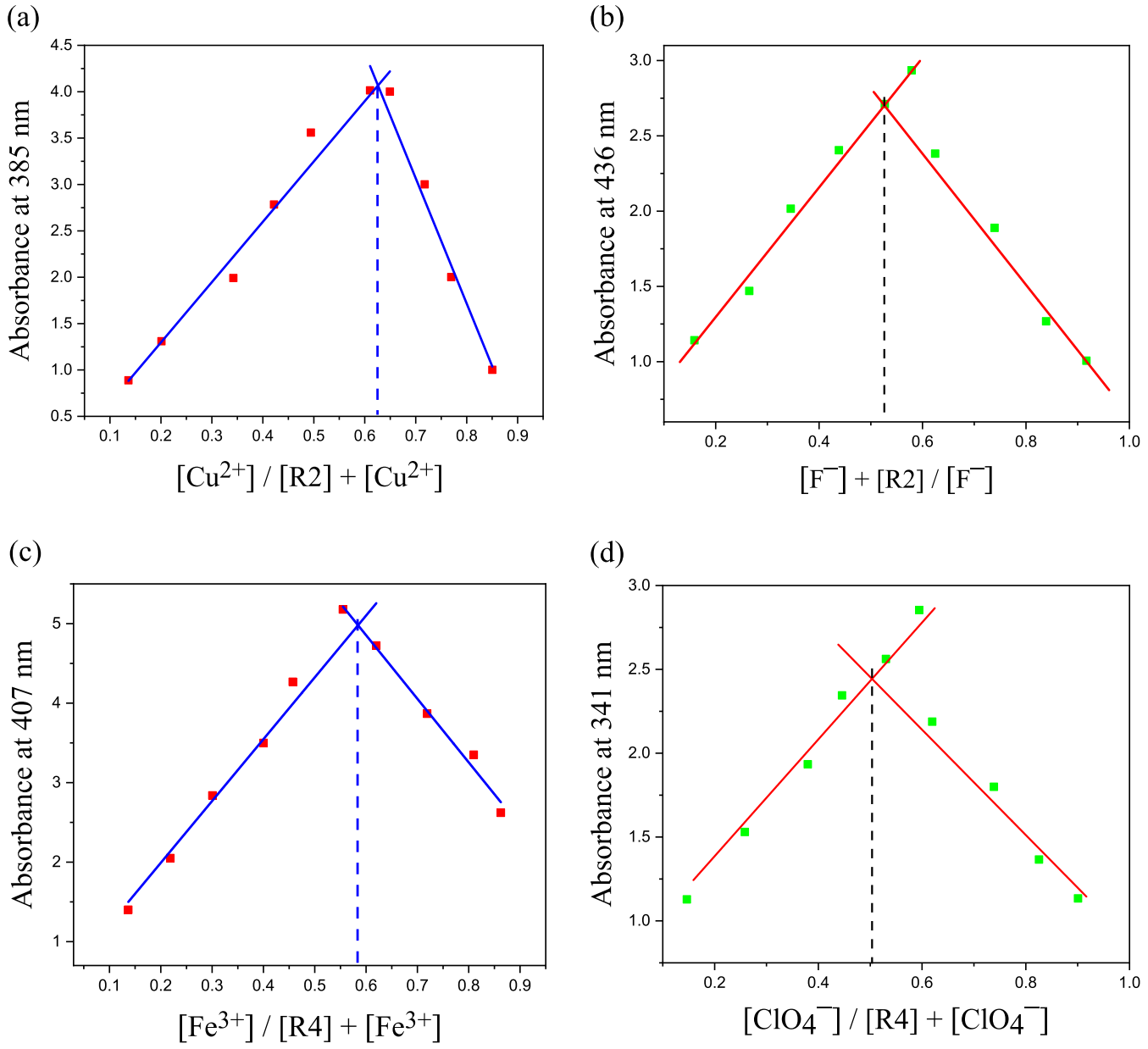

Figure 5. Job's plots for determining the stoichiometry of the probes with cations and anions in a CH_3CN:DMF (9:1 v/v) solution using absorption spectral studies: R2 + Cu^{2+} (a), R2 + F^- (b), R4 + Fe^{3+} (c), and R4 + ClO_4^- (d).

whereas R4 results in a decrease in the absorption intensity at 353 nm with the appearance of a new band at 421 nm. The addition of ClO_4^- anions to probe R1 results in a decrease in the absorption intensity at 278 and 310 nm with the appearance of a new band at 413 nm, and no appreciable change was observed with probe R2. The addition of ClO_4^- to R3 showed a bathochromic shift of 25 nm from 318 to 343 nm with an increase in the absorbance intensity, while R4 with ClO_4^- experienced a hypsochromic shift of 12 nm from 353 to 341 nm with a decrease in the absorbance intensity. The observed shift in the wavelength of the peaks was due to colorization of the probe solution and evidence of hydrogen bond stretching toward the probe−anion interaction. Thus, the probes (R1−R4) show sensing properties with F^- and ClO_4^- anions, whereas the rest of the anions tested displayed insignificant responses or showed trivial changes in a shift in wavelength/intensity of absorption due to their low affinity with probes, which indicates the selective sensing of F^-/ClO_4^- anions by all four probe molecules. Among the four probes (R1−R4), the probe−anion interaction was easily observed by R1 and R2. All probes exhibit authentic H-bonding and deprotonation with F^-/ClO_4^- anions due to N−H binding interactions. The sensing selectivity of F^-/ClO_4^- anions is in the order R2 > R1 > R3 ≃ R4.

To gain more insight into the binding characteristics, titrations were carried out with stepwise addition of sensed cations (Fe^{3+}/Cu^{2+}) and anions (F^-/ClO_4^-) to the probe molecules (R1−R4) at a concentration of 2.5−5.0 × 10^{-5} M, and the absorption spectra were obtained after each addition of analytes and calibration plots were plotted (Figures 2, 3, and S14−S17). From the UV−vis spectral titration data, the binding constants for probes with sensed ions were calculated using the Benesi−Hildebrand equation by plotting the changes in the absorbance against the concentration of the analyte, and the limit of detection and the binding stoichiometric ratio were

https://doi.org/10.1021/acsomega.4c04001
ACS Omega 2024, 9, 50957−50977

resolved using calibration and Job's plots, respectively (Figures 4, 5, S18, and S19 and Table 1). The probe R1 with ClO_4^- (R1 + ClO_4^-), R2 with Fe^{3+}, F^-, and ClO_4^- (R2 + Fe^{3+}/F^-/ClO_4^-), R3 with Fe^{3+} (R3 + Fe^{3+}), and R4 with Cu^{2+} (R4 + Cu^{2+}) show high binding constant values (2.60×10^6–7.44×10^6 M^{-1}) with a high magnitude and low limit of detection (0.11–0.80 μM) than the others. The selectivity and sensitivity of probe R4 were found to be efficacious toward Cu^{2+} cations with a lower limit of detection compared to the other sensed cations. Meanwhile, the isosbestic points at 398, 448, and 357 nm also confirmed the formation of complexes between probe R3 and Fe^{3+}/Cu^{2+} cations and between probe R4 and F^- anions, respectively. Job's plot analysis for the interaction between the probes and sensed cations (Cu^{2+}/Fe^{3+}) exhibited 1:2 binding stoichiometry, whereas that between probes and sensed anions (F^-/ClO_4^-) showed 1:1 binding stoichiometry by plotting absorption intensity versus equivalence of sensed ions. To better understand the complexation behavior of the probe molecules, MALDI-time-of-flight (TOF) mass analysis of the R3 + Cu^{2+} complex was carried out (Figure S20). The appearance of a peak at m/z 607.05 assignable to [R3 + $2Cu^{2+}$ + 4Cl] clearly supports the results of Job's plot analysis.

Table 1. Binding Constant, Limit of Detection, and Binding Stoichiometry of the Probes (R1–R4) toward Cations and Anions

sl. no.	probes + inorganic ions	binding constant (M^{-1})	limit of detection (μM)	binding stoichiometry
1	R1 + Fe^{3+}	3.43×10^5	0.21	1:2
2	R1 + Cu^{2+}	4.63×10^5	0.64	1:2
3	R1 + F^-	3.70×10^5	0.24	1:1
4	R1 + ClO_4^-	3.20×10^6	0.46	1:1
5	R2 + Fe^{3+}	2.60×10^6	0.18	1:2
6	R2 + Cu^{2+}	7.69×10^4	0.31	1:2
7	R2 + F^-	6.32×10^6	0.42	1:1
8	R2 + ClO_4^-	4.40×10^6	0.20	1:1
9	R3 + Fe^{3+}	3.01×10^6	0.80	1:2
10	R3 + Cu^{2+}	4.13×10^5	0.47	1:2
11	R3 + F^-	2.73×10^5	0.70	1:1
12	R3 + ClO_4^-	7.08×10^4	0.52	1:1
13	R4 + Fe^{3+}	3.15×10^5	0.13	1:2
14	R4 + Cu^{2+}	7.44×10^6	0.21	1:2
15	R4 + F^-	6.64×10^5	0.11	1:1
16	R4 + ClO_4^-	8.08×10^4	0.19	1:1

Fluorescence Responses with Cations and Anions. To gain deeper insight into the detection capabilities of the synthesized dual-responsive probes (R1–R4), fluorescence spectral titrations were carried out by adding cations and anions, both separately and simultaneously (Figures 6, 7, and S21). The fluorescence responses were investigated for the probe–cation (R1–R4 + Cu^{2+}), probe–anion (R1–R4 + F^-/ClO_4^-), and simultaneous addition of Cu^{2+} cations and ClO_4^- anions to probe R2 (R2 + Cu^{2+} + ClO_4^-) interactions. The probes (R1–R4) showed weak fluorescence emission at 400–508 nm upon excitation at 310–360 nm. Upon addition of the Cu^{2+} cations to R1–R4, the intensity of the emission bands at 468, 411, 431, and 422 nm increased by 10, 14, 02, and 15-fold, respectively, without any significant shift in the wavelength. Upon the addition of F^- to R1–R4, the intensity of the emission band increased by 13, 8, 6, and 21-fold, and upon the addition of ClO_4^- to R1–R4, the intensity of the emission band increased by 12, 7, 5, and 41-fold, respectively, without any significant shift in the wavelength. The observed increase in the fluorescence intensity could be due to the combination of intramolecular charge transfer (ICT) and chelation-enhanced fluorescence (CHEF) behavior.[27,28] These properties, along with the excitation wavelength and emission maxima, indicate excellent photophysical characteristics, including high fluorescence enhancement and Stokes shift, which support the sensing abilities of the synthesized probe molecules (Table S1). The fluorescence quantum yield (Φ) was determined for one probe molecule (R1) and its complexes (R1 + Cu^{2+}/F^-). Φ of R1 was found to be 0.010, which increased to 0.025 and 0.057 upon complexation with Cu^{2+} cations and F^- anions, respectively, further supporting the sensing capabilities of the synthesized probe molecules toward inorganic ions. In addition, upon simultaneous addition of Cu^{2+} cations followed by ClO_4^- anions to probe R2, the intensity of the emission band at 411 nm increased up to 11-fold, which supports the effective dual-responsive behavior of the probe. Furthermore, emission titrations were also performed with stepwise addition of Cu^{2+} cations and F^-/ClO_4^- anions to probes R1 and R2 at a concentration of 5×10^{-5} M, and the spectra were recorded for every addition of analytes, and the corresponding calibration plots were plotted. The binding constants for R4 + Cu^{2+} and R2 + F^- were estimated to be 7.44×10^6 and 6.32×10^6 M^{-1} with limits of detection of 0.21 and 0.42 μM, respectively (Figures S22–S24).

In order to explore the practical applications of the synthesized probes, we examined the pH effect, response time, and reversibility behaviors of the probes using fluorescence spectroscopy. The suitable pH range is one of the most significant factors for the recognition of inorganic ions in real applications; hence, the fluorescence intensity of probe R1 in the absence and presence of Cu^{2+} cations and F^- anions at various pH values (1.0–13.0) was measured. Probe R1 showed weak emission at 468 nm within the pH range, and no noticeable change in color was observed for free R1 in the pH range examined. Upon the addition of Cu^{2+}/F^- ions, significant color and spectral changes were observed for the R1 + Cu^{2+}/F^- complexes at all pH values (Figure 8a). The response of R1 + Cu^{2+}/F^- in the pH range of 6.0–10.0 is independent of the pH of the solution and exhibits maximum intensity. Hence, we chose CH_3CN:DMF (9:1, v/v, pH 7.1) as the solvent medium for our investigation. These results demonstrate that probe molecules can be used for the detection and determination of Cu^{2+}/F^- ions. To evaluate the real-time recognition of sensed ions and hence the stability of complex formation, the response time of probe R1 toward Cu^{2+} cations and F^- anions in a CH_3CN:DMF (9:1, v/v) solution was investigated (Figure 8b). The probe R1 interacted quickly with both ions, in which the color changed from colorless to reddish brown and greenish yellow upon the addition of a few drops of Cu^{2+} and F^- ions, respectively, in a very short time, with the formation of stable R1 + Cu^{2+}/F^- complexes. The fluorescence intensity of the R1 + Cu^{2+}/F^- complexes at 468 nm remained nearly constant throughout the analysis. The color of the complex solutions remained almost unchanged for several days under laboratory conditions. This indicates that the probe is highly sensitive to analytes and the complexes formed are also very stable.

The reversibility of the synthesized probes was studied using ethylenediaminetetraacetic acid (EDTA), a strong chelating agent, and probe R3 as a model compound (Figure 9). Probe R3 shows only weak fluorescence at 431 nm, and upon the addition

https://doi.org/10.1021/acsomega.4c04001
ACS Omega 2024, 9, 50957–50977

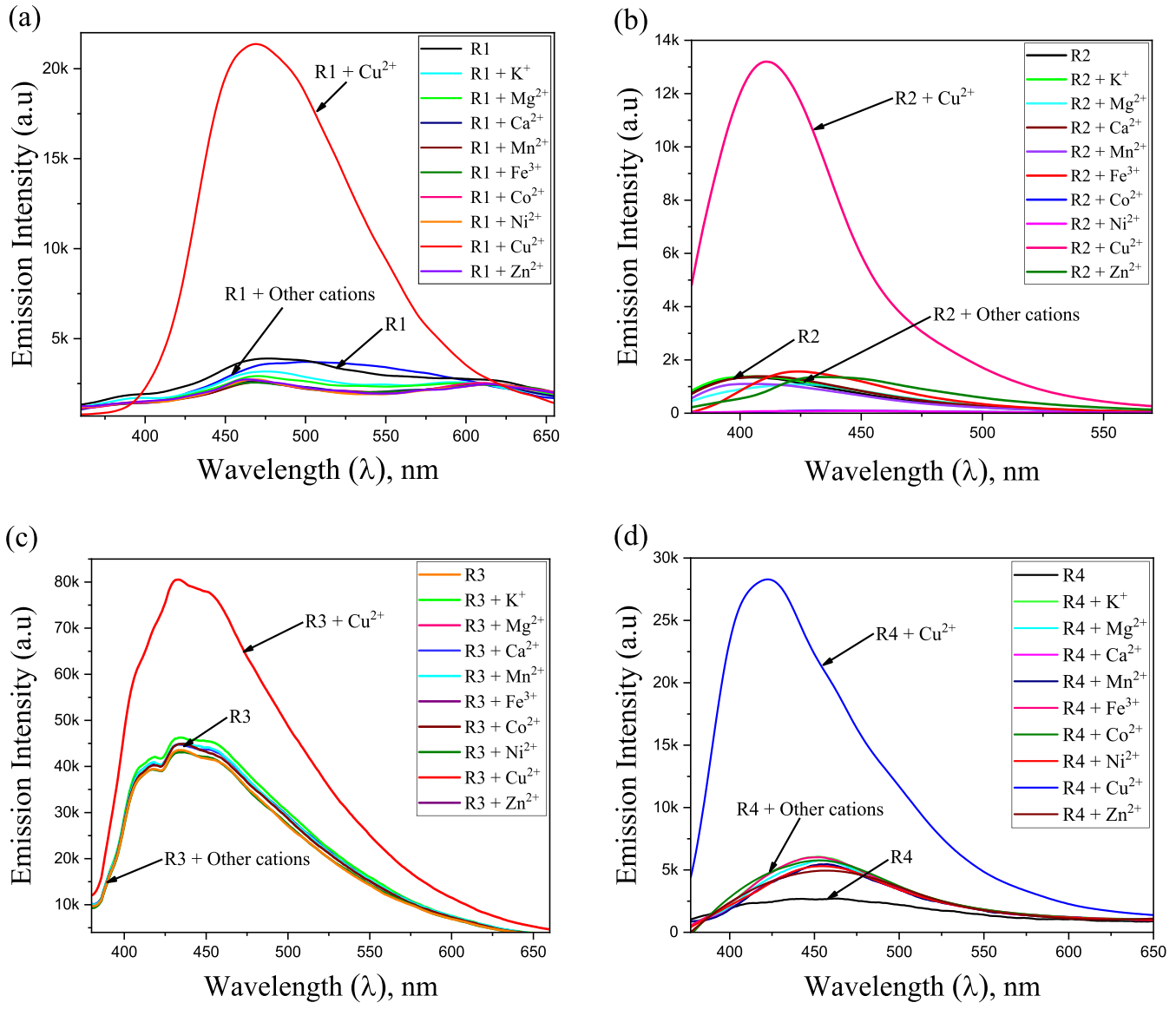

Figure 6. Emission spectral responses of probes R1 (a), R2 (b), R3 (c), and R4 (d) upon addition of various cations in CH_3CN:DMF (9:1 v/v) solution.

of Cu^{2+} cations to R3, the fluorescence emission intensity increased by 36-fold without a significant shift in the wavelength due to the formation of the R3 + Cu^{2+} complex. Upon the addition of 10 μM EDTA solution, the intensity was dramatically reduced due to the formation of nonfluorescent products (R3 and EDTA + Cu^{2+}). The original emission intensity was reversed by further addition of an equivalent amount of Cu^{2+} to this solution due to the formation of the R3 + Cu^{2+} complex. The changes in fluorescence intensity were found to be recyclable through the alternate addition of Cu^{2+} cations and EDTA. The titration was repeated five times, and the original spectrum was recovered each time. These results indicate that the coordination process is reversible with the sequential addition of Cu^{2+} cations and EDTA, and the probe molecules could be reused repeatedly as "off−on−off" sensors for the detection of cations.[29,30]

^{1}H NMR Titrations of Probes (R1−R4) with F^-/ClO_4^- Anions. To gain insight into the sensing mechanism of probe molecules toward sensed anions, NMR titration experiments were performed by sequential addition of F^-/ClO_4^- anions as tetrabutylammonium salts to R1−R4, which provided strong evidence for the probe−anion interaction (Figures 10 and S25−S27). It is quite challenging to predict complex formation involving hydrogen bonding or deprotonation by using the adequate basic strength of the guest molecule. Upon sequential addition (1−6 equiv) of F^- anions to probes R1 and R2, the intensity of the N−H signals at 11.64−10.39 ppm diminishes, which indicates the formation of hydrogen bonds between the probes and F^- anions; at higher equivalents, these signals vanish accompanied by a downfield shift of aromatic proton signals, whereas, upon the addition of ClO_4^- anions to R1 and R2, the intensity of these signals decreases with broadening at higher equivalents and disappears only in the case of R2. In the case of R3 and R4, upon sequential addition of F^- anions to the solution of probes, the intensity of indole −NH signals at 11.81−11.44 ppm and the intensity of N−H signals at 10.30−9.37 ppm disappear, which suggests deprotonation of these protons, whereas the addition of ClO_4^- anion to R3 and R4, the intensity of these signals decrease with a downfield shift and broadening at higher equivalents, and disappear only in the case of R4,

https://doi.org/10.1021/acsomega.4c04001
ACS Omega 2024, 9, 50957−50977

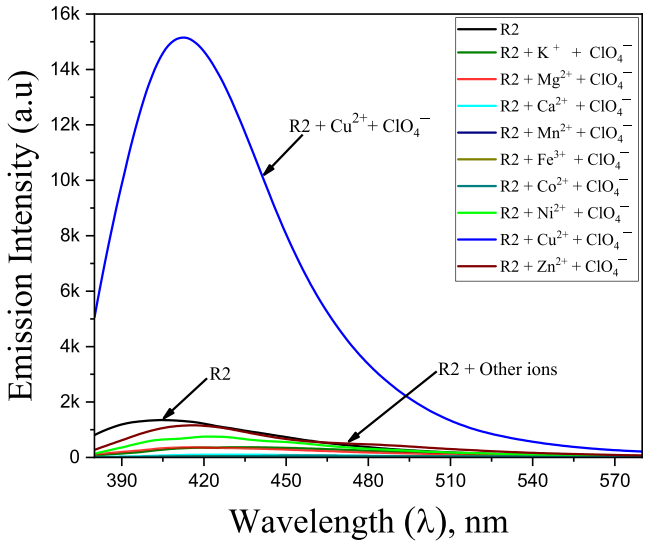

Figure 7. Emission spectral titrations of probe R2 upon simultaneous addition of cations followed by ClO_4^- anions.

suggesting the formation of H-bonding.[31] Besides, the aromatic protons also displayed prominent downfield chemical shifts. The observed chemical shifts are due to deprotonation, which results in increased electron density leading to enhanced ICT processes within the probe molecules.[1,32] These findings demonstrate that the probe molecules can sense F^-/ClO_4^- anions via the H-bonding/deprotonation mechanism.

Paper Strip Tests. The practical applicability of the probe molecules was ascertained using paper strip experiments by testing the sensing ability of R4 as a model compound. Whatman filter paper No. 40 (4 × 1 cm) was plugged with a solution of R4 (1.5×10^{-5} M) for 5 min and dried. Then, solutions of various concentrations (2.5×10^{-2} to 10^{-6} M) of ions were added to the pretreated paper strips of R4 (Figure 11). The R4-coated paper strips showed distinct color changes in the presence of the analyzed ions in solution, which decreased when moving toward lower concentrations. However, the color of R4-coated paper strips showed no noticeable color changes at a concentration of less than 10^{-5} M. The observed results demonstrated that the paper strip experiments can be used as a simple and operative technique for tracking the Fe^{3+}/Cu^{2+} cations and F^-/ClO_4^- anions in real samples, without any additional instruments.[33,34]

Theoretical Studies. *Geometry Optimization.* The binding and structural properties of compounds can be provided with exclusive information through molecular modeling, along with the energy-minimized conformation, in the absence of crystal data. In order to analyze the geometric parameters, such as bond length, bond angle, and binding ability of the compounds, theoretical calculations were carried out to obtain optimized structures of the compounds with inorganic ions, based on DFT studies using the B3LYP function with 631+G and LANL2DZ basis sets (Figures S28−S33 and Tables S2−S9). The optimized structures and structural parameters of the probes (R1−R4) and their binding with Fe^{3+}/Cu^{2+} cations and F^-/ClO_4^- anions indicate the significant contribution of −NH/O/N/S atoms in sensing inorganic cations and anions. The C═O bond distances of R1 and R3 increase from 1.205 and 1.288 Å to 1.612 and 1.491 Å, respectively, upon binding with Fe^{3+}, and increase to 1.341 and 1.682 Å, respectively, upon binding with Cu^{2+} ions. In the case of R2 and R4, the C═S bond distances increase from 1.582 and 1.348 Å to 1.828 and 1.490 Å, respectively, upon binding with Fe^{3+}, and increase to 1.853 and 1.682 Å, respectively, upon binding with Cu^{2+} ions. The C═N bond length values of R1−R4 obtained in the range of 1.245−1.463 Å increase to 1.310−1.606 and 1.410−1.620 Å, after binding with Fe^{3+} and Cu^{2+} ions, respectively. The increase in bond lengths of C═O, C═S, and C═N after binding with Fe^{3+} and Cu^{2+} cations indicate the sensing of these ions by probe molecules.[35,36] The calculated N−H bond lengths of R1−R4 are obtained in the range of 1.033−1.049 Å, indicating a single bond between nitrogen and hydrogen atoms, which increases to 1.316−1.543 and 1.219−1.523 Å, after binding with F^- and ClO_4^- anions, respectively, indicating the formation of hydrogen bond upon sensing of F^-/ClO_4^- anions by the probe molecules.[37]

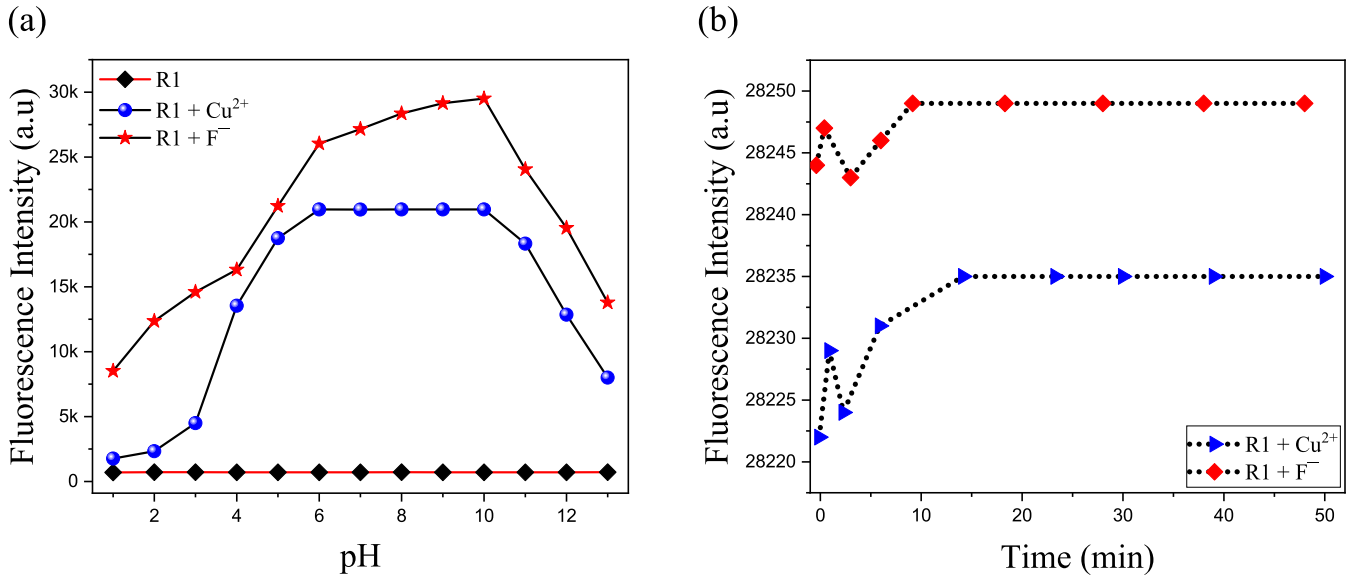

Figure 8. Effect of pH on the fluorescence responses of R1 + Cu^{2+} and R1 + F^- complexes (a), and the response time of probe R1 toward Cu^{2+} cations and F^- anions (b), in a CH_3CN:DMF (9:1, v/v) solution.

https://doi.org/10.1021/acsomega.4c04001
ACS Omega 2024, 9, 50957−50977

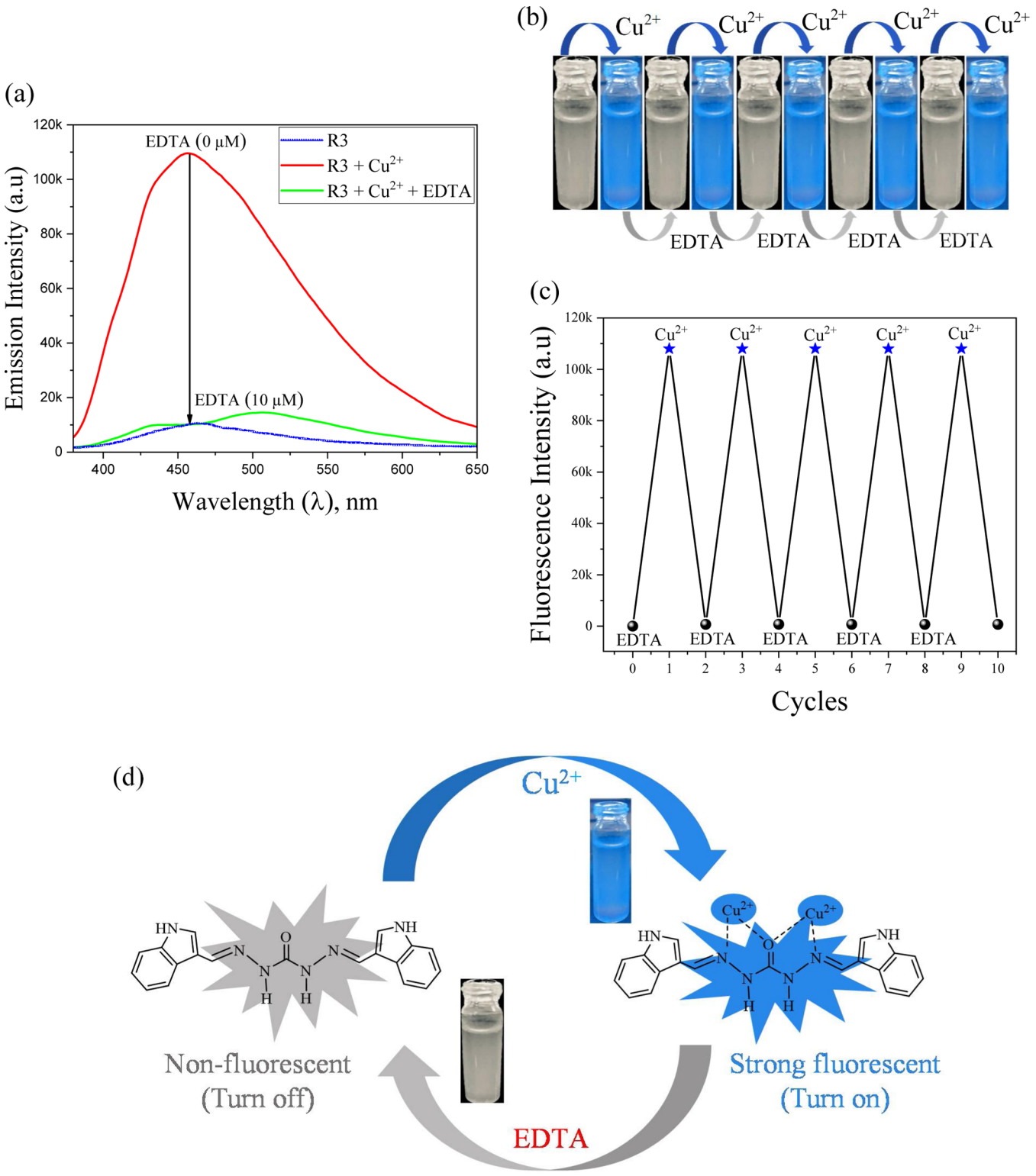

Figure 9. Fluorescence reversible interaction of probe R3 upon alternative addition of Cu^{2+} cations and EDTA (a), photograph showing the alternative addition of Cu^{2+} cations and EDTA (b), number of reversible cycles for the alternative addition of Cu^{2+} cations and EDTA (c), and the proposed detection mechanism of the "turn on−turn off" on fluorescence response of R3 (d).

The calculated bond angles (°) within the probe molecules (R1−R4) display reductions and increments subsequent to their interaction with sensed ions (Fe^{3+}/Cu^{3+} cations and F^{-}/ClO_4^{-} anions). Upon binding of Fe^{3+} and Cu^{3+} cations to R1 and R3, noticeable changes in the bond angles are observed. The variations in bond angles of C6−N7−H22, N7−N8−O11, C9−N8−O10, and C9−N10−O10 were 1.97, 4.91, 4.06, and 6.10, and 3.47, 6.97, 6.68 and 3.69, respectively, when R1 and R3 bind with Fe^{3+} and Cu^{2+} cations, and those of C6−N7−H22, C9−N10−H24, and N10−N12−H25 were 2.42, 2.68, and 2.20, and 8.40, 6.97, and 2.90, respectively, when R2 and R4 bind with Fe^{3+} and Cu^{2+} cations. After the interaction of the metal ions

https://doi.org/10.1021/acsomega.4c04001
ACS Omega 2024, 9, 50957−50977

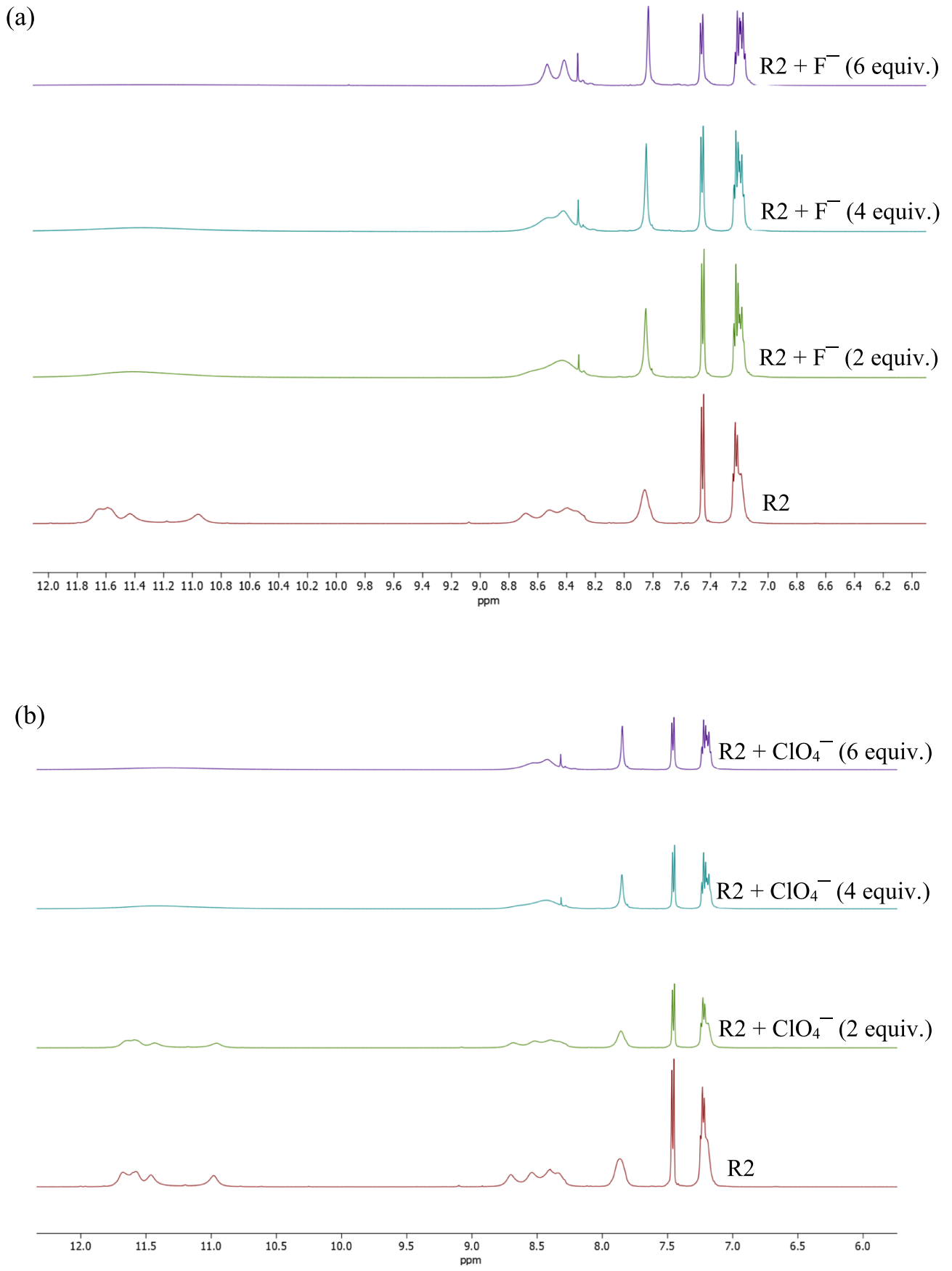

Figure 10. Partial ^{1}H NMR spectra of R2, and sequential addition of F^{-} (a) and ClO_4^{-} (b) anions to R2.

https://doi.org/10.1021/acsomega.4c04001
ACS Omega 2024, 9, 50957−50977

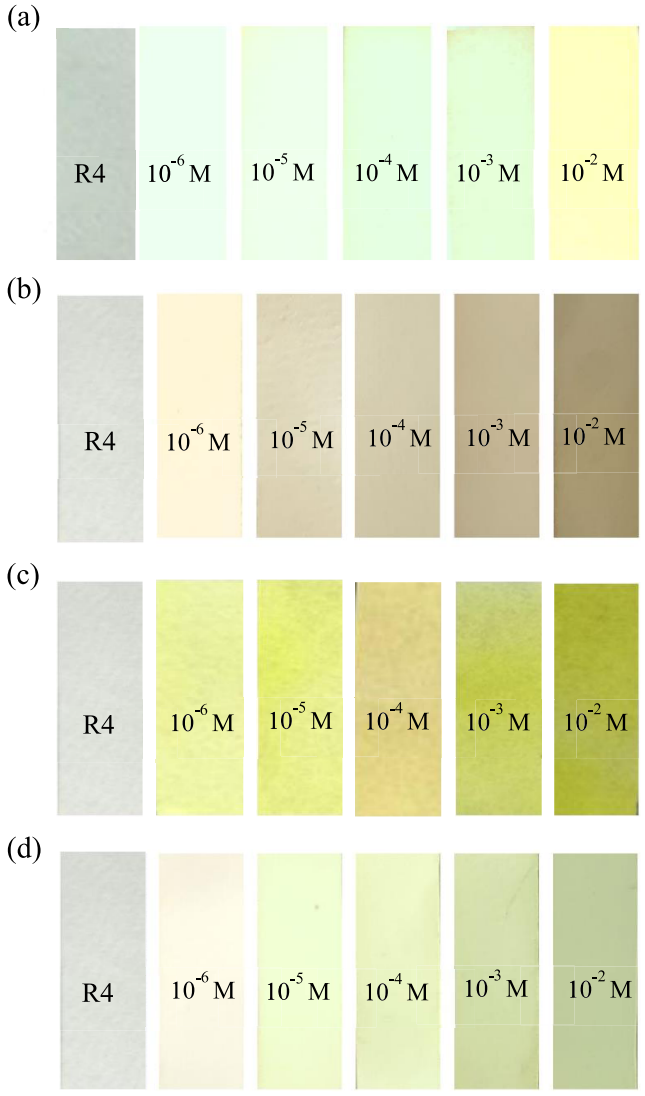

Figure 11. Photographs of paper strips of probe R4 upon addition of Fe^{3+} (a), Cu^{2+} (b), F^- (c), and ClO_4^- (d) ions at different concentrations.

with probes, clear binding through C═O/C═S and C═N is evidenced by oxygen, sulfur, and nitrogen atoms. The variation in the bond angles of C9−N8−H23, C9−N10−H24, C13−N12−H34, and C13−N14−H35 are found to be between 1.05 and 4.77 when the probes bind with F^- anions, and between 1.05 and 3.23 when the probes bind with ClO_4^- anions. The changes in bond angles indicate the hydrogen bonding interaction between the N−H and the sensed anions.[38]

Frontier Molecular Orbital (FMO) Analysis. In frontier molecular orbital (FMO) analysis, the lowest unoccupied molecular orbital (LUMO) reflects the ability to gain an electron, while the highest occupied molecular orbital (HOMO) reflects the electron-donating ability. The FMOs for probe molecules (R1−R4), R1−R4 + Fe^{3+}/Cu^{2+}, and R1−R4 + F^-/ClO_4^- were measured to analyze the energy gap and electron transfer mechanism within the probes (Figures 12 and S34−S38 and Table S10). The HOMO is the orbital that primarily acts as an electron donor, while the LUMO is the orbital that primarily acts as an electron acceptor and compounds with low HOMO−LUMO energy gaps exhibit significant intramolecular charge transfer (ICT), which helps to predict the stability and reactivity of molecules.[39,40] The E_{HOMO} and E_{LUMO} energy values were derived from the orbital energy level analysis of probes (R1−R4), R1−R4 + Fe^{3+}/Cu^{2+}, and R1−R4 + F^-/ClO_4^-. The ΔE values of R1−R4 are found to be between 0.1209 and 0.1472, which upon binding with Fe^{3+} and Cu^{2+} cations decrease to 0.0831−0.1051 and 0.0990−0.1238 eV, respectively, and to 0.1139−0.1304 and 0.0882−0.1272 eV, respectively, upon binding with F^- and ClO_4^- anions. The small energy gap in the molecules indicates higher reactivity and offers electrons easily, which means they are easier to charge transfer than molecules with a large energy gap. The ΔE values of probe molecules after binding with sensed ions are found to be less than those of the free probes and are in good agreement with the results obtained from the optical spectra with respect to the shift in wavelength. These results provide additional evidence for the binding mode of the probe molecules with sensed cations and anions.

Plausible Sensing Mechanism. Based on the spectral and theoretical studies, the possible coordination mode and sensing mechanism of the probe molecules (R1−R4) with sensed cations and anions have been proposed (Figure 13). As the probe molecules have different binding sites, it was necessary to examine the effect of the F^-/ClO_4^- anions on the binding ability of the probes for cations and vice versa. Optical studies were performed in two different ways: first, the probes were titrated with sensed metal ions and anions individually, followed by the simultaneous addition of sensed cations (Cu^{2+}/Fe^{3+}) and anions (F^-/ClO_4^-). Low fluorescence responses were observed for the probes due to the photoinduced electron transfer effect. In contrast, an increase in fluorescence intensity was observed with the addition of sensed inorganic ions due to the chelation-enhanced fluorescence effect. The notable changes observed in the fluorescence studies highlight the dual-responsive nature of the synthesized probe molecules. ^1H NMR titration studies provide strong evidence for the sensing of F^-/ClO_4^- anions and the H-bonding/deprotonation of the NH protons of the probe molecules. Further, the dual-sensing behavior of the probe molecules observed in the experimental studies was also supported by the theoretical studies, where significant changes in the bond length and bond angle indicated the same sensing behavior.

Toxicity Assessment. In order to investigate the potential application of the fluorescent probes (R1−R4) and Cu^{2+} cations in the *Dr*G cell line and zebrafish larvae, the toxicity of the probe molecules was evaluated. *DrG* cells treated with probes did not show morphological changes up to 20 μM mL^{-1} after 24 h of exposure (Figure S39). At higher concentrations (80 μM mL^{-1}) of probes R2 and R4, 65% cell death was observed in the *Dr*G cell line.

In Vitro Cytotoxicity by MTT and NR Assays. Cytotoxicity assessment by MTT and NR assays showed the viability of *Dr*G cells when treated with probes (R1−R4) at concentrations up to 80 μM mL^{-1} for 24 h. Varying concentrations of probes between 5 and 80 μM mL^{-1} were employed for *in vitro* cytotoxicity assays in zebrafish gill cell lines using two standard endpoints (Figure S40). In the case of R2 and R4, the highest concentration (80 μM mL^{-1}) was found to be toxic, and less toxicity was observed for R1 and R3; however, at lower concentrations (up to 20 μM mL^{-1}), all probes were not significantly cytotoxic to *Dr*G cells compared to the control cells. Thus, a progressive increase in the concentration of probes leads to an increase in toxicity when compared to control cells.

https://doi.org/10.1021/acsomega.4c04001
ACS Omega 2024, 9, 50957−50977

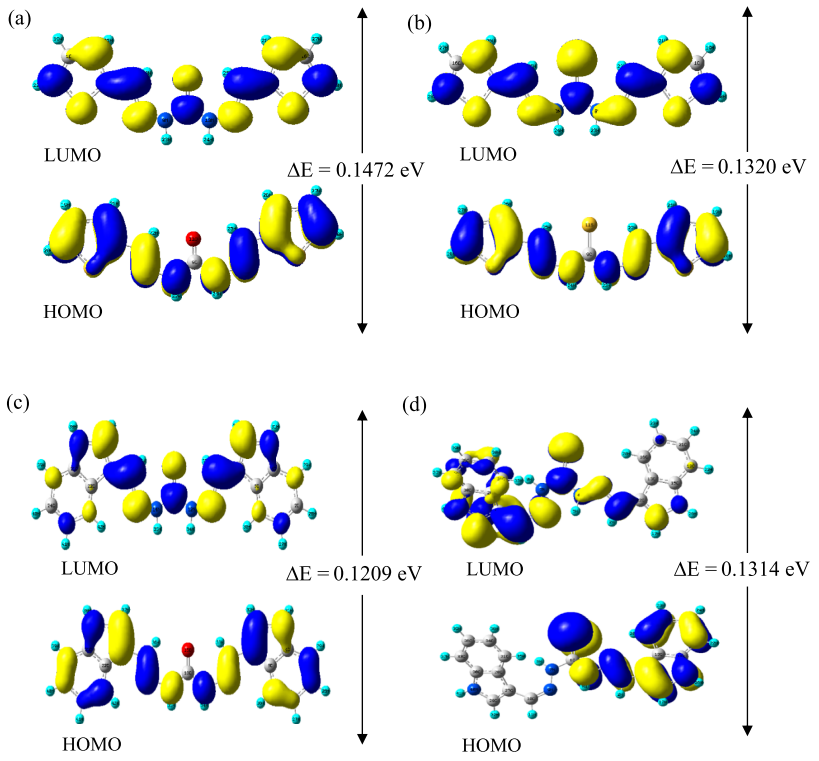

Figure 12. Frontier molecular orbitals of probes R1 (a), R2 (b), R3 (c), and R4 (d).

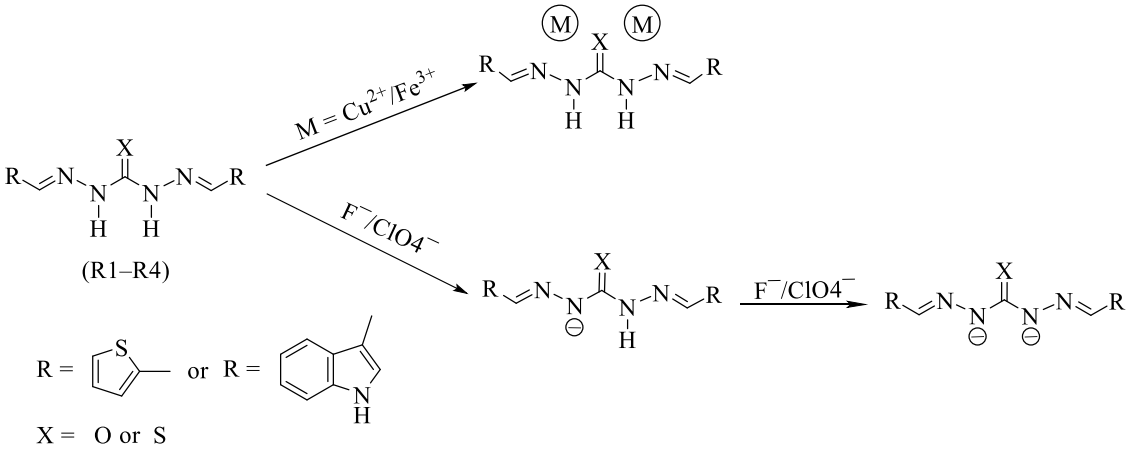

Figure 13. Plausible sensing mechanism of the dual-responsive probes (R1 and R4) in the presence of sensed cations and anions.

In Vitro Recognition of Cu^{2+} Cations in Live Cells. The intracellular distribution of Cu^{2+} cations and the probe's ability to reach the cell membranes were investigated using fluorescence microscopy (Figure 14). In order to ascertain the intracellular Cu^{2+} cations, exponentially growing *Dr*G cells were incubated with Cu^{2+} cations (20 μM mL^{-1}) at 28 °C for 30 min, and then washed with PBS to remove excess Cu^{2+} cations. For fluorescence detection of intracellular Cu^{2+} cations, cells were incubated with serum-free medium (2 mL) containing 10 and 20 μM mL^{-1} R1−R4 (10 mM stock solution prepared in DMSO and diluted in culture media) for 30 min. The cells were rinsed with three additional PBS washes before imaging. Fluorescence microscopy images of *Dr*G cells showed high levels of blue fluorescence in the cytoplasm. The obvious blue fluorescence signal may be due to the complexation of probe molecules with Cu^{2+} cations (R1−R4 + Cu^{2+}) in the *Dr*G cells. Intracellular imaging of *Dr*G cells treated with R1−R4 alone revealed no fluorescence by fluorescence microscopy. These results indicate that the probe molecules can diffuse cell membranes, allowing for visualization of the intracellular distribution of Cu^{2+} cations in *Dr*G cells.[41]

In Vivo Recognition of Cu^{2+} Cations in Zebrafish Larvae. To assess the suitability of the probes (R1−R4) for *in vivo* applications, we investigated their ability to detect Cu^{2+} cations in zebrafish larvae (Figure 15). Zebrafish larvae are widely used as model organisms for *in vivo* bioimaging of metal ions due to their small size and transparency.[42−44] The blue fluorescence resulting from R1−R4 + Cu^{2+} complexes is distinctly visible in the anterior region of the larvae. Upon examining the images of the fish head and eyes revealed that blue fluorescence was present throughout the body. These results indicate that the probes have the potential to serve as Cu^{2+} sensors in living organisms. Similar results were also observed when the 3-day-old zebrafish larvae were exposed to Al^{3+} and thiophene-3-

https://doi.org/10.1021/acsomega.4c04001
ACS Omega 2024, 9, 50957−50977

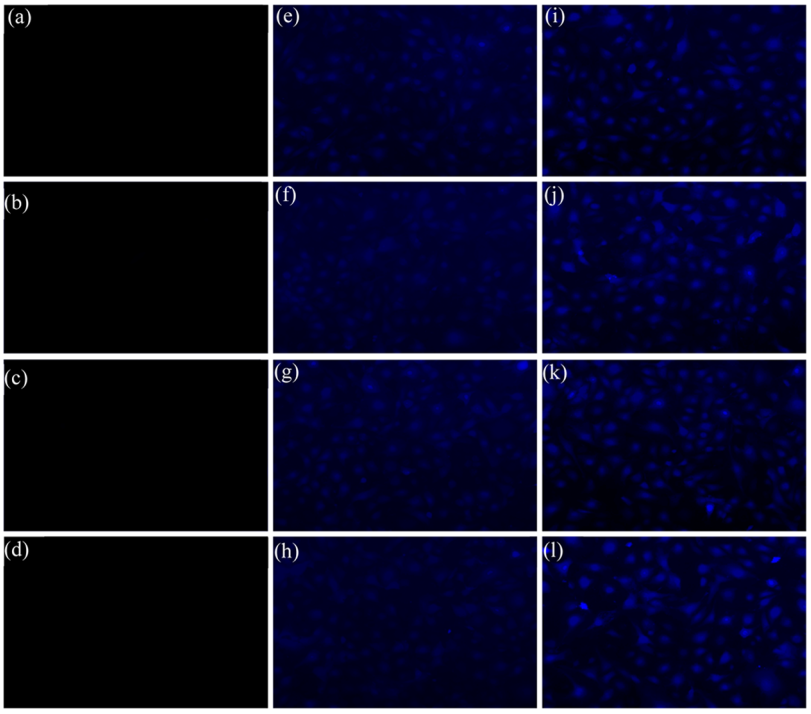

Figure 14. Fluorescence photographs of the *Dr*G cell line upon incubation with probes R1 (a), R2 (b), R3 (c), and R4 (d) alone for 30 min as a control, incubation with 10 μM of R1 (e), R2 (f), R3 (g), and R4 (h) for 30 min, followed by incubation with 20 μM of Cu^{2+} cations for 30 min, and incubation with 20 μM of R1 (i), R2 (j), R3 (k), and R4 (l) for 30 min, followed by incubation with 20 μM of Cu^{2+} cations. All of the fluorescence microphotographs were captured at 100× magnification.

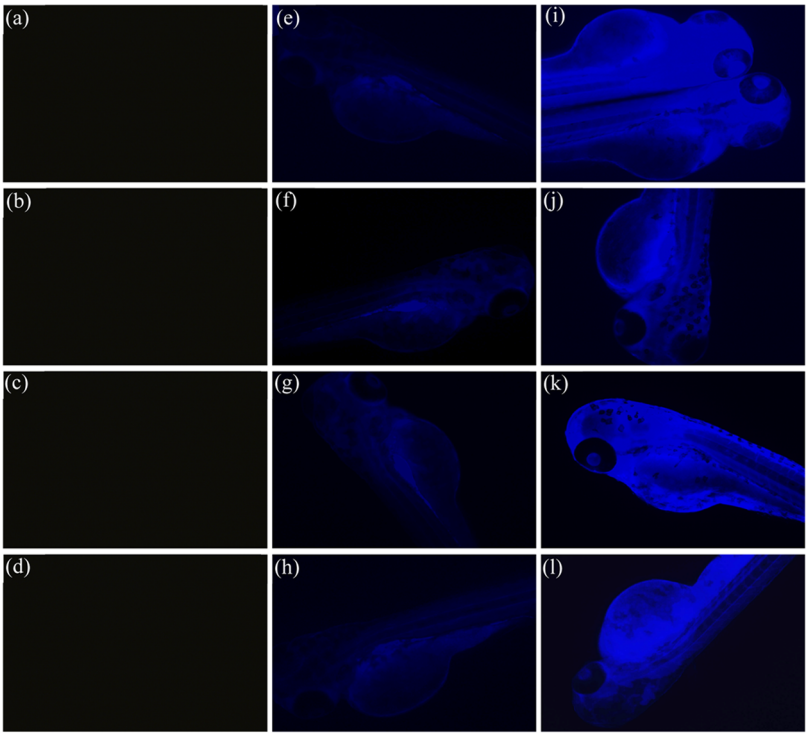

Figure 15. Fluorescence photographs of the newly hatched zebrafish larvae upon incubation with probes R1 (a), R2 (b), R3 (c), and R4 (d) alone for 30 min as a control, incubation with 10 μM of R1 (e), R2 (f), R3 (g), and R4 (h) for 30 min, followed by incubation with 20 μM of Cu^{2+} cations for 30 min, and incubation with 20 μM of R1 (i), R2 (j), R3 (k), and R4 (l) for 30 min, followed by incubation with 20 μM of Cu^{2+} cations. All of the fluorescence images were captured at 40× magnification.

carbohydrazide probe, in which the blue fluorescence dots were clearly observed in the zebrafish head and digestive tract due to the formation of probe-Al^{3+} complex.[25]

Molecular Logic Gates. Molecular logic gates are the second most leading application and the fundamental components of any kind of electronic or digital device.[17,45] In general, logic

https://doi.org/10.1021/acsomega.4c04001
ACS Omega 2024, 9, 50957−50977

(a)

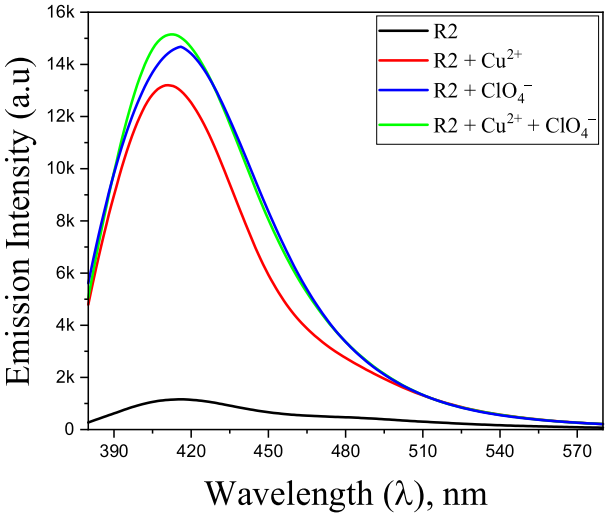

(b)

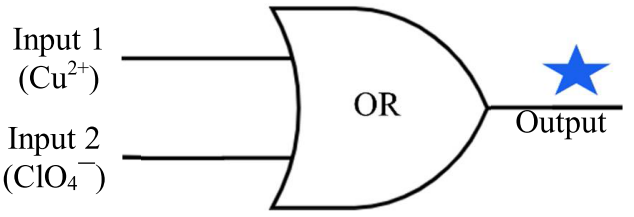

(c)

S. No	Input 1 (Cu^{2+})	Input 2 (ClO_4^-)	Output (λ_{emi} = 411 nm)
1	0	0	0
2	1	0	1
3	0	1	1
4	1	1	1

(d)

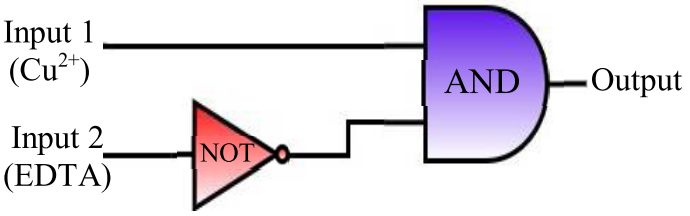

(e)

S. No	Input 1 (Cu^{2+})	Input 2 (EDTA)	Output (λ_{emi} = 431 nm)
1	0	0	0
2	1	0	1
3	0	1	0
4	1	1	0

Figure 16. Fluorescence spectral titrations of probe R2 upon addition of Cu^{2+} cations, ClO_4^- anions, and simultaneous addition of Cu^{2+} cations and ClO_4^- anions (a), molecular logic circuit for probe R2 and truth table for OR logic gate (b, c), and molecular logic circuit for probe R3 and truth table for INHIBIT logic gate (d, e), derived from fluorescence data.

circuit outputs are derived from chemically encoded information as inputs and their emission properties as outputs (Figure 16). It is possible to design different molecular logic circuits, for example, (i) the INHIBIT logic circuit with an AND logic gate and (ii) the combination of NOT logic gates based on the truth table. Since the fluorescence response of the probes is distinctly affected by the addition of both cations and anions, we used a binary logic function with Cu^{2+} and ClO_4^- ions as dual stimulating inputs, and fluorescence as outputs. The logic function of the OR gate, which is one of the basic gates from which all other functions can be constructed, is normally switched on if either one or both inputs are turned on. As a consequence of the observed emission shift of probe R2 in the presence of Cu^{2+} and ClO_4^- ions, an OR gate can be easily interpreted by utilizing Cu^{2+} and ClO_4^- ions as input signals, along with the corresponding emission as the output. Boolean operations are typically used to depict this system, where high emission intensity values are ON (1), and low emission intensity values are OFF (0). The fluorescence emission at 411 nm could be at a high value when either one or both inputs (Cu^{2+} and ClO_4^-) are present, and the output would be zero only when all inputs are in the low state.[46] The truth table supports the OR logical behavior of probe R2. The truth table is also designed with fluorescence spectra for two chemical inputs, Cu^{2+} and EDTA, to probe R3, which supports an INHIBIT logic gate. The combined logic gate was motivated by the reversible and reproducible interaction between R3 + Cu^{2+} and EDTA, along with the resulting changes in the emission intensity. Four ionic inputs were used to construct INHIBIT logic gates using fluorescence output signals. There was an increase in fluorescence emission after the addition of Cu^{2+} ions, indicating fluorescence ON.

Comparison of Synthesized Probes with Other Similar Reported Probes. A comparison of the present probe molecules

https://doi.org/10.1021/acsomega.4c04001
ACS Omega 2024, 9, 50957−50977

with other carbohydrazone/thiocarbohydrazone-based probe molecules reported in the literature is presented in Table S11. To the best of our knowledge, unlike our probe molecules, there are only a limited number of reports in which a single probe is used as a dual-sensor molecule. Even though each probe molecule showed some advantages with respect to the solvent used, sensitivity, naked-eye detection, and applications, the present probe molecules exhibit quite distinctive analytical features with respect to their ease of synthesis, dual-sensing behavior, detection limit, and application in live-cell imaging.[47−51]

CONCLUSIONS

In summary, we developed four dual-responsive chromogenic/fluorogenic probe molecules (R1−R4) with three binding sites for the detection of inorganic ions in solution. These probes exhibited selective and sensitive responses to metal ions (Fe^{3+}/Cu^{2+}) and anions (F^-/ClO_4^-) at micromolar concentrations, as confirmed by spectral techniques and further supported by theoretical calculations. The sensing of F^-/ClO_4^- anions is attributed to H−bonding and deprotonation of the NH protons of the carbohydrazone/thiocarbohydrazone moiety. The probes could be regenerated from their complexes, as evidenced by the reversibility of the reaction with EDTA. The potential applications of the synthesized probe molecules are demonstrated with paper strip experiments for the detection of sensed ions in real samples, in addition to bioimaging and molecular logic function studies. The probes were effectively employed for bioimaging of Cu^{2+} cations, which were clearly observed in the anterior part of larvae, offering strong probes for live-cell imaging to examine chemical signaling in complex multicellular systems. Further, INHIBIT molecular logic gates for the detection of inorganic ions were developed using fluorescence data. The key findings of this work have inspired us to focus on future research by modifying the design strategy to develop sensor molecules to be used as fluorescent markers for ion sensing in human cancer cells, and we are now engaged in the tuning of the spacer and efficient fluorophores with respect to the development of novel probe molecules.

ASSOCIATED CONTENT

Supporting Information

The Supporting Information is available free of charge at https://pubs.acs.org/doi/10.1021/acsomega.4c04001.

FT-IR spectroscopy, absorption, colorimetric, emission, ^1H and ^{13}C NMR spectroscopy, sensor titrations, DFT calculations, bioimages, MTT, and NR assays. (PDF)

AUTHOR INFORMATION

Corresponding Author

Aziz Kalilur Rahiman − *Post-Graduate and Research Department of Chemistry, The New College, University of Madras, Chennai 600014, India;* orcid.org/0000-0002-0824-0493; Email: akrahmanjkr@gmail.com, kalilurrahiman@thenewcollege.edu.in

Authors

Ramalingam Gajendhiran − *Post-Graduate and Research Department of Chemistry, The New College, University of Madras, Chennai 600014, India*

Abbas Khaja Raees Ahmed − *Post-Graduate and Research Department of Chemistry, The New College, University of Madras, Chennai 600014, India;* orcid.org/0009-0002-2737-3707

Sivaraj Mithra − *Post-Graduate and Research Department of Zoology, Aquatic Animal Health Laboratory, C. Abdul Hakeem College, Melvisharam 632509, India*

Seepoo Abdul Majeed − *Post-Graduate and Research Department of Zoology, Aquatic Animal Health Laboratory, C. Abdul Hakeem College, Melvisharam 632509, India*

Azeez Sait Sahul Hameed − *Post-Graduate and Research Department of Zoology, Aquatic Animal Health Laboratory, C. Abdul Hakeem College, Melvisharam 632509, India*

Kesavan Muthu − *Interdisciplinary Institute of Indian System of Medicine, SRM Institute of Science and Technology, Chennai 603203, India*

Sankar Sarathkumar − *Department of Physical Chemistry, University of Madras, Chennai 600025, India*

Selvan Nehru − *Department of Physical Chemistry, University of Madras, Chennai 600025, India;* orcid.org/0000-0001-7998-3705

Complete contact information is available at: https://pubs.acs.org/10.1021/acsomega.4c04001

Author Contributions

R.G. designed and performed the research, interpreted the data, and wrote the original draft, with oversight from all other authors. A.K.R.A. contributed to the data interpretation. S.M., S.A.M., and A.S.S.H. contributed to the resources, formal analysis, and data curation. K.M. performed formal analysis and data curation. S.S. and S.N. contributed to the software and performed validation. A.K.R. contributed to the conceptualization, methodology, validation, and writing of the review and editing.

Notes

The authors declare no competing financial interest.

ACKNOWLEDGMENTS

R.G. gratefully acknowledges the State Government of Tamil Nadu, India, for providing a financial annual research assistance grant (G.O. (Ms.) No. 96./25-11-2021). S.M., S.A.M., and A.S.S.H. thank the Department of Biotechnology, New Delhi, India, for partial support with the imaging work (Project Nos. BT/PR40452/NDB/39/750/2020 and BT/PR41899/AAQ/3/1006/2021).

REFERENCES

(1) Bose, P.; Ghosh, P. Visible and near-infrared sensing of fluoride by indole conjugated urea/thiourea ligands. *Chem. Commun.* **2010**, *46*, 2962−2964.

(2) Singh, G.; Tamana; Sharma, D.; Mithun; Kaur, H.; Rani, B.; Khan, S. A.; Radha, A.; Singh, K. N. Luminescent Schiff base derived triazolyl silane: An emerging sensor for detection of Fe^{3+}, Cu^{2+} and a ceruloplasmin inducer validated via docking. *J. Photochem. Photobiol. A* **2024**, *448*, No. 115329.

(3) Kaur, N.; Gauri. Anthraquinone appended chemosensors for fluorescence monitoring of anions and/or metal ions. *Inorg. Chim. Acta* **2022**, *536*, No. 120917.

(4) Amuthakala, S.; Bharathi, S.; Rahiman, A. K. Semicarbazone and thiosemicarbazone appended 4-diethylamino-2-hydroxybenzyl compounds as highly selective bifunctional chemosensors: An experimental and computational approach. *Inorg. Chim. Acta* **2023**, *546*, No. 121302.

(5) Kundu, A.; Hariharan, P. S.; Prabakaran, K.; Anthony, S. P. Developing new Schiff base molecules for selective colorimetric sensing of Fe^{3+} and Cu^{2+} metal ions: Substituent selectivity and color change. *Sens. Actuators, B* **2015**, *206*, 524−530.

(6) Santos-Figueroa, L. E.; Moragues, M. E.; Raposo, M. M. M.; Batista, R. M. F.; Martinez-Manez, R.; et al. Synthesis and evaluation of fluorimetric and colorimetric chemosensors for anions based on (oligo)thienyl-thiosemicarbazones. *Tetrahedron* **2012**, *68*, 7179−7186.
(7) Chang, Y.; Li, B.; Mei, H.; Yang, L.; Xu, K.; Pang, X. Indole-based colori/fluorimetric probe for selective detection of Cu^{2+} and application in living cell imaging. *Spectrochim. Acta, Part A* **2020**, *226*, No. 117631.
(8) Kuwar, A.; Patil, R.; Singh, A.; Sahoo, S. K.; Marek, J.; Singh, N. A two-in-one dual channel chemosensor for Fe^{2+} and Cu^{2+} with nanomolar detection mimicking IMPLICATION logic gate. *J. Mater. Chem. C* **2014**, *3*, 453−460.
(9) Murugan, A. S.; Vidhyalakshmi, N.; Ramesh, U.; Annaraj, J. *In vivo* bio-imaging studies of highly selective, sensitive rhodamine based fluorescent chemosensor for the detection of Cu^{2+}/Fe^{3+} ions. *Sens. Actuators, B* **2018**, *274*, 22−29.
(10) Alhaddad, M.; El-Sheikh, S. M. Selective and fast detection of fluoride-contaminated water based on a novel salen-Co-MOF chemosensor. *ACS Omega* **2021**, *6*, 15182−15191.
(11) Kumar, R.; Kumar, S. P.; Singh, P.; Hundal, G.; Hundal, M. S.; Kumar, S. A fluorescent chemosensor for detection of perchlorate ions in water. *Analyst* **2012**, *137*, 4913−4916.
(12) Singh, P.; Mittal, L. S.; Vanita, V.; Kumar, R.; Bhargava, G.; Waliab, A.; Kumar, S. Bay functionalized perylenediimide as a deaggregation based intracellular fluorescent probe for perchlorate. *Chem. Commun.* **2014**, *50*, 13994−13997.
(13) Gale, P. A. Synthetic indole, carbazole, biindole and indolocarbazole-based receptors: Applications in anion complexation and sensing. *Chem. Commun.* **2008**, *38*, 4525−4540.
(14) Jeyanthi, D.; Iniya, M.; Krishnaveni, K.; Chellappa, D. Novel indole based dual responsive "turn-on" chemosensor for fluoride ion detection. *Spectrochim. Acta, Part A* **2015**, *136*, 1269−1274.
(15) Maity, D.; Govindaraju, T. Highly selective visible and near-IR sensing of Cu^{2+} based on thiourea−salicylaldehyde coordination in aqueous media. *Chem. Eur. J.* **2011**, *17*, 1410−1414.
(16) Hijji, Y. M.; Barare, B.; Kennedy, A. P.; Butcher, R. Synthesis and photophysical characterization of Schiff base as anion sensor. *Sens. Actuators, B* **2009**, *136*, 297−302.
(17) Das, B.; Jana, A.; Mahaptra, A. D.; Chattopadhyay, D.; Dhara, A.; Mabhai, S.; Sey, S. Fluorescein derived Schiff base as fluorimetric zinc(II) sensor via 'turn on' response and its application in live cell imaging. *Spectrochim. Acta, Part A* **2019**, *212*, 222−231.
(18) Das, B.; Dey, S.; Maiti, G. P.; Bhattacharjee, A.; Dhara, A.; Jana, A. Hydrazinopyrimidine derived novel Al^{3+} chemosensor: Molecular logic gate and biological applications. *New J. Chem.* **2018**, *42*, 9424−9435.
(19) Mohammadi, A.; Kianfar, M. A simple colorimetric chemosensor with highly performance for detection of cyanide and copper ions and its practical application in real samples. *J. Photochem. Photobiol. A* **2018**, *367*, 22−31.
(20) Aatif, A. M.; Kumar, R. S.; Joseph, S.; Vetriarasu, V.; Majeed, S. A.; Kumar, S. K. A. Pyridine carbohydrazide-based fluorescent chemosensor for In^{3+} ion and its applications in water samples. live cells, and zebrafish imaging. *J. Photochem. Photobiol., A* **2023**, *434*, No. 114257.
(21) Mosmann, T. Rapid colorimetric assay for cellular growth and survival: Application to proliferation and cytotoxicity assays. *J. Immunol. Methods* **1983**, *65*, 55−63.
(22) Brüschweiler, B. J.; Wiirglerb, F. E.; Fent, K. Cytotoxicity *in vitro* of organotin compounds to fish hepatoma cells PLHC-1 (*Poeciliopsis lucida*). *Aquat. Toxicol.* **1995**, *32*, 143−160.
(23) Krone, P.; Blechinger, S.; Evans, T.; Ryan, J.; Noonan, E.; Hightower, L. Use of fish liver PLHC-1 cells and zebrafish embryos in cytotoxicity assays. *Methods* **2005**, *35*, 176−187.
(24) Ryan, J. A.; Hightower, L. E. Evaluation of heavy metal ion toxicity in fish cells using a combined stress and cytotoxicity assay. *Environ. Toxicol. Chem.* **1994**, *13*, 1231−1240.
(25) Venkateswarulu, M.; Gambhir, D.; Kaur, H.; Daniel, P. V.; Mondal, P.; Koner, R. R. A long-range emissive mega-Stokes inorganic−organic hybrid material with peripheral carboxyl functionality for As(V) recognition and its application in bioimaging. *Dalton Trans.* **2017**, *46*, 13118−13125.
(26) Tian, H.; Qiao, X.; Zhang, Z.; Xie, C.; Li, Q.; Xu, J. A high performance 2-hydroxynaphthalene Schiff base fluorescent chemosensor for Al^{3+} and its applications in imaging of living cells and zebrafish *in vivo*. *Spectrochim. Acta, Part A* **2019**, *207*, 31−38.
(27) Tang, L.; Zhou, P.; Zhang, Q.; Huang, Z.; Zhao, J.; Cai, M. A simple quinoline derivatized thiosemicarbazone as a colorimetic and fluorescent sensor for relay recognition of Cu^{2+} and sulfide in aqueous solution. *Inorg. Chem. Commun.* **2013**, *36*, 100−104.
(28) Santhiya, K.; Mathivanan, M.; Tharmalingam, B.; Anitha, O.; Ghorai, S.; Natarajan, R.; Murugesapandian, B. A new 7-(diethylamino)coumarin and 4-(diethylamino)phenol appended unsymmetrical thiocarbohydrazone: Detection of moisture in organic solvent and sequential fluorimetric detection of Cu^{2+} ions and cysteine. *J. Photochem. Photobiol. A* **2022**, *432*, 114105.
(29) Kumar, G. G. V.; Kesavan, M. P.; Sivaraman, G.; Annaraj, J.; Anitha, K.; Tamilselvi, A.; Athimoolam, S.; Sridhar, B.; Rajesh, J. Reversible NIR fluorescent probes for Cu^{2+} ions detection and its living cell imaging. *Sens. Actuators, B* **2018**, *225*, 3235−3247.
(30) Sarma, S.; Devi, B.; Bhattacharyya, P. K.; Das, D. K. Condensation product of p-anisaldehyde and L-phenylalanine: Fluorescent "on-off" sensor for Cu^{2+} and IMPLICATION logic gate. *J. Fluoresc.* **2020**, *30*, 1513−15218.
(31) Grover, N.; Sankar, M. N-Confused porphyrin−A unique 'turn on' chemosensor for CN^- and F^- ions and 'turn off' sensor for ClO_4^- ions. *Chem. Asian. J.* **2020**, *15*, 2192−2197.
(32) Saini, N.; Prigyai, N.; Wannasiri, C.; Ervithayasuporn, V.; Kiatkamjornwong, S. Green synthesis of fluorescent N,O-chelating hydrazone Schiff base for multi-analyte sensing in Cu^{2+}, CN^- and F^- ions. *J. Photochem. Photobiol. A* **2018**, *358*, 215−225.
(33) Amuthakala, S.; Selvan, D. S. A.; Rahiman, A. K. 4−Functionalized terpyridine derivative as dual responsive chemosensor for biologically important inorganic cations and fluoride anion. *J. Iran. Chem. Soc.* **2020**, *17*, 1237−1248.
(34) Goswami, N.; Gogoi, H. P.; Barman, P. A hydrazine-based unsymmetrical bis-imine-Schiff base as a chemosensor for turn-off fluorescence and naked-eye detection of Cu^{2+} ion: Application in aqueous media using test strips. *J. Photochem. Photobiol. A* **2024**, *446*, No. 115106.
(35) Jayasudha, P.; Manivannan, R.; Elango, K. P. Simple colorimetric chemodosimeters for selective sensing of cyanide ion in aqueous solution via termination of ICT transition by Michael addition. *Sens. Actuators, B* **2015**, *221*, 1441−1448.
(36) Basheer, S. M.; Willis, A. C.; Sreekanth, A. Spectroscopic and TD-DFT studies on the turn-off fluorescent chemosensor based on anthraldehyde N(4) cyclohexyl thiosemicarbazone for the selective recognition of fluoride and copper ions. *J. Lumin.* **2017**, *183*, 266−280.
(37) Parsaee, Z.; Haratipour, P.; Lariche, M. J.; Vojood, A. A novel high performance nano chemosensor for copper(II) ion based on an ultrasound-assisted synthesized diphenylamine-based Schiff base: Design, fabrication and density functional theory calculations. *Ultrason. Sonochem.* **2018**, *41*, 337−349.
(38) Islam, M.; Hameed, A.; Ayub, K.; Naseer, M. M.; Hussain, J.; Alharthy, R. D.; Asari, A.; et al. Receptor-spacer-fluorophore based coumarin-thiosemicarbazones as anion chemosensors with 'turn on' response: Spectroscopic and computational (DFT) studies. *ChemistrySelect* **2018**, *3*, 7633−7642.
(39) He, X.; Xu, W.; Xu, C.; Ding, F.; Chen, H.; Shen, J. Reversible spiropyran-based chemosensor with pH-switches and application for bioimaging in living cells. *Pseudomonas aeruginosa* and zebrafish. *Dyes Pigm.* **2020**, *180*, 108−497.
(40) Golbedaghi, R.; Justino, L. L. G.; Bahrampour, M.; Fausto, R. A novel fluorescent chemosensor for Cu^{2+} ion based on a new hexadentate ligand receptor: X-ray single crystal of the perchlorate salt of the ligand, ion selectivity assays and TD-DFT study. *Inorg. Chim. Acta* **2021**, *515*, No. 120061.

https://doi.org/10.1021/acsomega.4c04001
ACS Omega 2024, 9, 50957−50977

(41) Li, Y.; Niu, Q.; Wei, T.; Li, T. Novel thiophene-based colorimetric and fluorescent turn-on sensor for highly sensitive and selective simultaneous detection of Al^{3+} and Zn^{2+} in water and food samples and its application in bioimaging. *Anal. Chim. Acta* **2019**, *1049*, 196−212.
(42) Yang, Y.-K.; Ko, S. K.; Shin, I.; Tae, J. Synthesis of a highly metal-selective rhodamine-based probe and its use for the *in vivo* monitoring of mercury. *Nat. Protoc.* **2007**, *2*, 1740−1745.
(43) Ma, X.; Wang, J.; Shan, Q.; Tan, Z.; Wei, G.; Wei, D.; Du, Y. A 'turn on' fluorescent Hg^{2+} chemosensor based on Ferrier carbocyclization. *Org. Lett.* **2012**, *14* (3), 820−823.
(44) Peng, J.; Xu, W.; Teoh, C. L.; Han, S.; Kim, B.; Samanta, A.; Er, J. C.; Wang, L.; Yuan, L.; Liu, X.; Chang, Y. T. High-efficiency *in vitro* and *in vivo* detection of Zn^{2+} by dye-assembled upconversion nanoparticles. *J. Am. Chem. Soc.* **2015**, *137* (6), 2336−2342.
(45) Paul, S.; Choudhury, A. R.; Dey, N. Dual-mode multiple ion sensing via analyte-specific modulation of keto-enol tautomerization of an ESIPT active pyrene derivative: Experimental findings and computational rationalization. *ACS Omega* **2023**, *8*, 6349−6360.
(46) Wang, S.; Men, G.; Zhao, L.; Hou, Q.; Jiang, S. Binaphthyl-derived salicylidene Schiff base for dual-channel sensing of Cu, Zn cations and integrated molecular logic gates. *Sens. Actuators, B* **2010**, *145*, 826−831.
(47) Devaraj, S.; Saravanakumar, D.; Kandaswamy, M. Dual responsive chemosensors for anion and cation: Synthesis and studies of selective chemosensor for F^- and Cu(II) ions. *Sens. Actuators, B* **2009**, *136*, 13−19.
(48) Kaur, K.; Bhardwaj, V. K.; Kaur, N.; Sing, N. Fluorescent chemosensor for Al^{3+} and resultant complex as a chemosensor for perchlorate anion: First molecular security keypad lick based on Al^{3+} and ClO_4^- inputs. *Inorg. Chem. Commun.* **2012**, *26*, 31−36.
(49) Sharma, S.; Hundal, M. S.; Hundal, G. Selective recognition of fluoride ions through fluorimetric and colorimetric response of a first mesitylene based dipodal sensor employing thiosemicarbazones. *Tetrahedron* **2013**, *54*, 2423−2427.
(50) Nakwanich, B.; Koonwong, A.; Suramitr, A.; Prompinit, P.; Pooarporn, R. P.; Hannongbua, S.; Suramitr, S. Spectroscopy and a theoretical study of colorimetric sensing of fluoride ions by salisylidene based Schiff base derivatives. *J. Mol. Struct.* **2021**, *1245*, No. 131132.
(51) Gümrah, Ö.; Gucoglu, M.; Satirouglu, N. Smartphone-assisted chemosensor based on thiocarbohydrazide Schiff base for selective detection of Hg^{2+} and Cu^{2+} ions. *J. Mol. Struct.* **2024**, *1316*, No. 138859.

https://doi.org/10.1021/acsomega.4c04001
ACS Omega 2024, 9, 50957−50977